ZIRAT18 ANNUAL REPORT

Annual Report

Authors

Peter Rudling
ANT International, Mölnlycke, Sweden

Friedrich Garzarolli
Fürth, Germany

David Franklin
Las Vegas, NV, USA

Ron Adamson
Fremont, CA, USA

A.N.T. INTERNATIONAL®

Advanced Nuclear Technology International
Analysvägen 5, SE-435 33 Mölnlycke
Sweden

info@antinternational.com
www.antinternational.com

Ecolabelled printed matter, 441 799

Disclaimer

The information presented in this report has been compiled and analysed by Advanced Nuclear Technology International Europe AB (ANT International®) and its subcontractors. ANT International has exercised due diligence in this work, but does not warrant the accuracy or completeness of the information. ANT International does not assume any responsibility for any consequences as a result of the use of the information for any party, except a warranty for reasonable technical skill, which is limited to the amount paid for this assignment by each ZIRAT/IZNA programme member.

Contents

1 Introduction (Peter Rudling)

The objective of the Annual Review of ZIRconium Alloy Technology (ZIRAT) and Information on Zirconium Alloys (IZNA) is to review and evaluate the latest developments in ZIRAT as they apply to nuclear fuel design and performance.

The objective is met through a review and evaluation of the most recent data on zirconium alloys and to identify the most important new information and discuss its significance in relation to fuel performance now and in the future. Included in the review are topics on materials research and development, fabrication, component design, and in-reactor performance presented in conferences, journals and reports.

The primary issues addressed in the review and this report is zirconium alloy research and development, fabrication, component design, ex- and in-reactor performance including:

- Regulatory bodies and utility perspectives related to fuel performance issues, fuel vendor developments of new fuel design to meet the fuel performance issues.
- Fabrication and Quality Control (QC) of zirconium manufacturing, zirconium alloy systems.
- Mechanical properties and their test methods (that are not covered in any other section in the report).
- Dimensional stability (growth and creep).
- Primary coolant chemistry and its effect on zirconium alloy component performance.
- Corrosion and hydriding mechanisms and performance of commercial alloys.
- Cladding primary failures.
- Post-failure degradation of failed fuel.
- Cladding performance in postulated accidents (Loss of Coolant Accident (LOCA), Reactivity Initiated Accident (RIA)).
- Dry storage.
- Potential Burnup (BU) limitations.
- Current uncertainties and issues needing solution are identified throughout the report.

Background data from prior periods have been included wherever needed. The data published in this Report is only from non-proprietary sources; however, their compilation, evaluations, and conclusions in the report are proprietary to ANT International and ZIRAT/IZNA members as noted on the title page.

The authors of the report are Dr. Ron Adamson, Mr. Friedrich Garzarolli, Dr. David Franklin, and, Mr. Peter Rudling, President of ANT International.

The work reported herein will be presented in two Seminars: in Clearwater Beach, FL., USA (February 10–12, 2013), in Bilbao, Spain (March 10–12, 2013).

The Term of ZIRAT18/IZNA13 started on February 1, 2013 and ends on March 31, 2014.

All literature that we refer to in this Report are available in the ANT International Literature Database (LDB).

2 BU achievements and key fuel performance issues (Peter Rudling)

2.1 Introduction

The objective of this section is to summarize the key performance issues that could affect fuel design, fabrication or operation of the nuclear fuel in the near term or the longer term. The information sources reviewed, screened and evaluated include nearly all the related publications and technical meeting presentations of the past, approximately 18 months and focuses primarily on extended BU data but also other key results are provided. The section is intended to be a guide to significant, current issues and provide an alert to items that could affect fuel related operations. The extensive volume of information involved limits the presentations to the most significant features and conclusions, and the reader is urged to refer to the referenced publications.

2.2 Trends in fuel operating conditions

2.2.1 General trends

Improved fuel reliability and operating economics are the driving forces for the changes in operating conditions, while maintaining acceptable margins to operating and regulatory safety limits. These are incentives for significant advances in materials technology, software for modelling fuel performance, sophisticated instrumentation and methods for post-irradiation examinations. Some of these advances in technology have increased the demands on fuel performance levels and put pressure on the regulatory bodies to license operations to increased BU levels. The types of changes in Light Water Reactor (LWR) operating methods intended to achieve improved safety and economics have not changed in the past years and still include:

- *Annual fuel cycles extended to 18 and 24 months,*
- *Increased discharge BUs to 58 GWD/MT batch average exposures by higher enrichments, increased number of burnable absorbers in the assemblies and in Pressurized Water Reactors (PWRs) higher Li and B levels in the coolant, or enriched B in the coolant,*
- *Plant power uprates that range from 2 to 20%,*
- *More aggressive fuel management methods with increased enrichment levels and peaking factors,*
- *Reduced activity transport by Zn injection into the coolant,*
- *Improved water chemistry controls and increased monitoring,*
- *Component life extension with Hydrogen Water Chemistry (HWC) and Noble Metal Chemistry (NMC)/On Line Noble Chemistry (OLNC) in Boiling Water Reactors (BWRs).*

2.2.2 Fuel cycles

Cycle lengths

The trend for increased fuel cycle lengths has come to a near "equilibrium" ***in the US*** *with PWRs operating at an average of 500 Effective Full Power Days (EFPD) per cycle and BWRs an average of 620 EFPD per cycle, up to a maximum of about 680 days for PWRs and 720 days for BWRs. Nearly all the US BWRs are trending toward 24 month cycles. The older, lower power density PWRs have implemented the 24 month cycles, but fuel management limitations, specifically the reload batch sizes required, have limited implementation of 24 month cycles in the high power density plants. The economics of 24 month cycles tend to become plant specific since they depend on the balance of a variety of plant specific parameters. The potential economic gains for cycle extension have decreased in the US as the downtimes for reloading and maintenance procedures were significantly reduced.*

Other countries *that historically have had only one peak power demand per year in the winter, compared to the two summer and winter power peaks in the US, are also trending toward longer cycles as a result of changes in economics, maintenance practices and licensing procedures. PWRs are trending toward 18 month cycles in France, Belgium and Germany.*

2.2.3 BU extension

The major incentive for extended BUs is the potentially improved fuel cycle economy. The improved economics depend in part on the decreased amount of spent FAs to be purchased and handled. This is balanced by the increased amount of uranium and enrichment services required. The economics of decreased assemblies could also be impacted by the much longer cooling times required for High Burnup (HB) and Mixed Oxide (MOX) fuels in spent fuel pools prior to on-site dry storage or transport to a storage facility.

The average batch BUs in US PWRs are currently in the range of 42-54 GWD/MT and in US BWRs in the range of 45-52 GWD/MT.

Some European plants operated in the 50-60 GWD/MT batch BU range and have designed to go to 62 GWD/MT in their current cycles in both PWRs and BWRs. This is feasible, in part, due to their greater margin to their regulatory BU limits. The maximum BU Lead Test Assemblies (LTAs) are in the range of 67 – 79 GWD/MT for both reactor types. BU ranges by countries are compared to their regulatory limits in Table 2-1.

In addition to potential technical issues, the two major constraints to higher BU are the regulatory limits noted in Table 2-1 and the 5% enrichment limit.

Table 2-1: Maximum BUs achieved vs. regulatory limits, (excludes LTAs).

	BU (GWD/MT)				
Country	**Batch**	**Assembly**	**Rod**	**Pellet**	**Regulatory limit**
USA	54	58	62	73	62.5 peak rod
Belgium		50-55			55 UO_2 assy., 50 MOX assy.
Czech Republic	51	56	61		60 peak rod
Finland	45.6	46.5	53		45 assy
France	47	51 UO_2 42 MOX			52 assy
Germany	58	62	68		65 assy
Hungary		50	62		
Japan	50	55	62		55 UO_2 assy., 45 MOX assy.
Korean Republic	46				60 rod
Netherlands	51.5	58	64.5		60 rod
Russia	60	65			
Spain	50.4	57.4	61.7	69	
Sweden	47	57.2	63.6		60 assy., 64 rod
Switzerland	58	60	65	71	80 pellet
Taiwan					60 rod (P), 54 assy. (B)
UK	44.3	46.5	50		55 pellet
Ukraine		50			

ANT International, 2011

Fortum's goal is to move to a 4 -batch loading scheme with TVEL fuel for both Loviisa NPP reactor units [Lindroth, 2013]. To achieve this goal the U-235 enrichment was increased from 4% to 4.37% and six Gd_2O_3 doped rods were added to the fuel assembly. These design changes increased the hot subchannel enthalpy rise but addition of mixing vanes in the spacer grids has restored the thermal margins. Previous tests in the Halden test reactor and hot cell and poolside examinations of high burnup TVEL assemblies with peak burnup of 53.4 MWd/kgU at Loviisa NPP revealed nothing that would prevent the irradiation of TVEL fuel assemblies up to 57 MWd/kgU. Fortum received Radiation and Nuclear Safety Authority's (STUK) approval for the assembly average burnup extension from 45 to 57 MWd/kgU for the 2nd generation Assemblies in July 2011. First full reload of 2nd generation assemblies was loaded for the 4th cycle in 2012 for Loviisa-1. Loviisa-2 is coming one year after.

2.3 Fuel reliability

[Lindroth, 2013] reported on fuel reliability activities in Loviisa NPP reactor units. The average fuel failure rate in Loviisa NPP has been 3.5×10^{-5} failed fuel rods per year (assuming that there is only one failed rod in a failed assembly) up to the refuelling outage in 2012 (Figure 2-1). There were about 20 operating cycles without any leaks from 1999 to 2008 and as of 2008, there has been only three defected rods that will be inspected to determine the failure cause (root cause examinations is a requirements of the Finish regulators, STUK).

The number of irradiation cycles of failed fuel assemblies at the time of the failure are presented in the Figure 2-2. The failure root causes are shown in Figure 2-3.

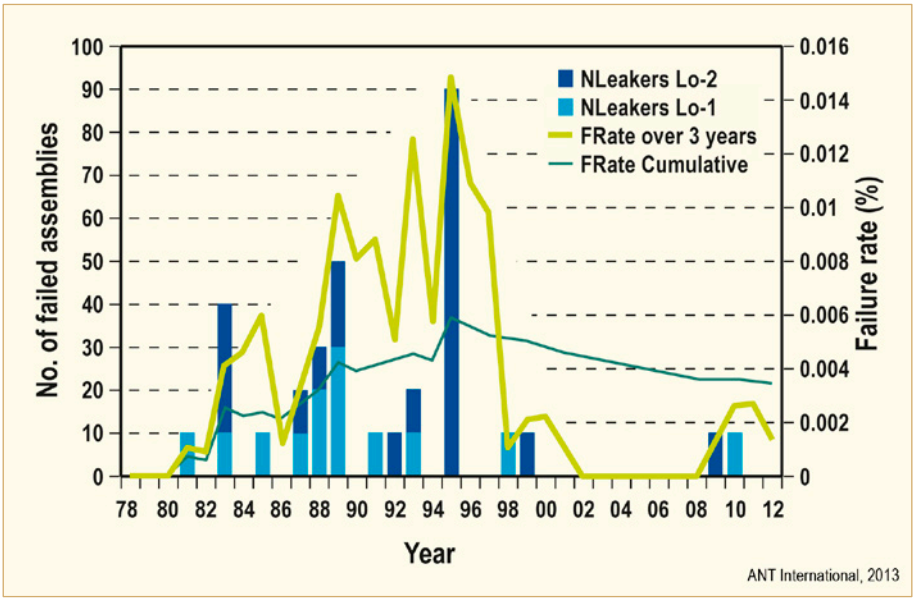

Figure 2-1: Fuel rod failure rate at Loviisa NPP 1978 – 2012, after [Lindroth, 2013].

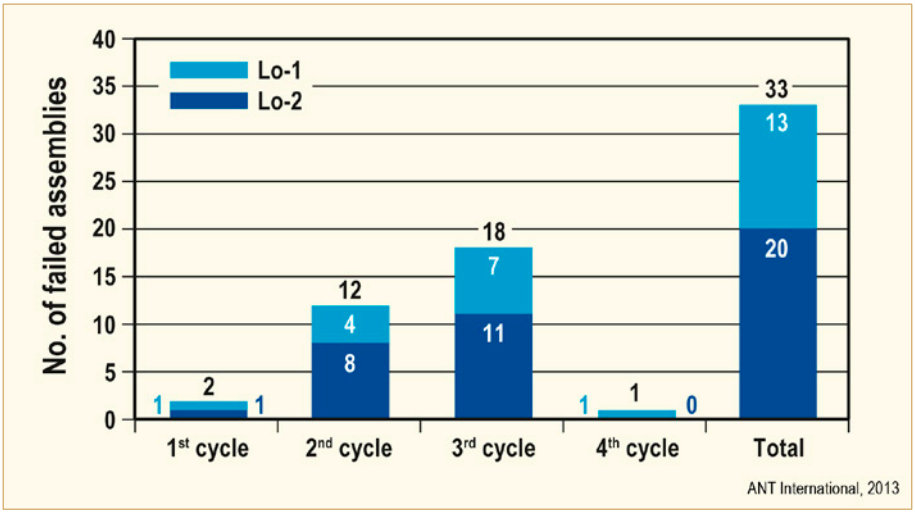

Figure 2-2: Fuel failures until August 2012 at Loviisa NPP, after [Lindroth, 2013].

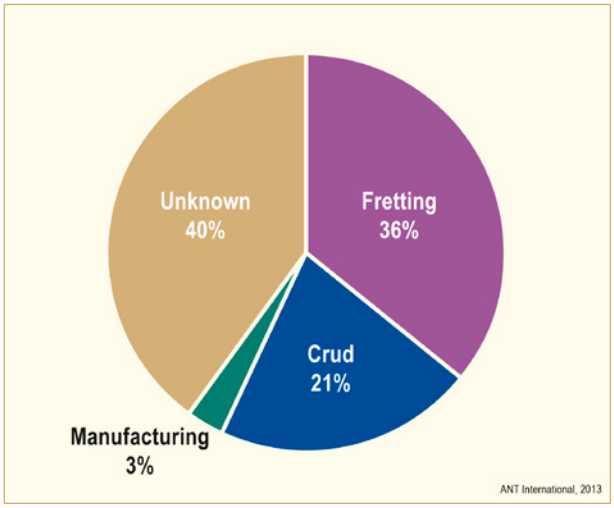

Figure 2-3: Fuel failure causes at Loviisa NPP (3 leakers from the years 2008 - 2012 are not yet examined and are missing from the figure), after [Lindroth, 2013].

2.4 New fuel designs

2.4.1 Korea nuclear fuel

[Kim, 2013] presented an interesting review of PWR fuel design development, the steps involved in verification of a new design as well as the new fuel designs emerging on the market.

Figure 2-4 and Figure 2-5 shows that the main fuel failure causes in Korea was PCI and excessive Zry-4 cladding corrosion from 2002 to 2006 while it changed to debris fretting in recent years when Zry-4 was replaced by ZIRLO. Table 2-2 summarizes the action taken by the nuclear industry to eliminate/minimize the fuel failure issues.

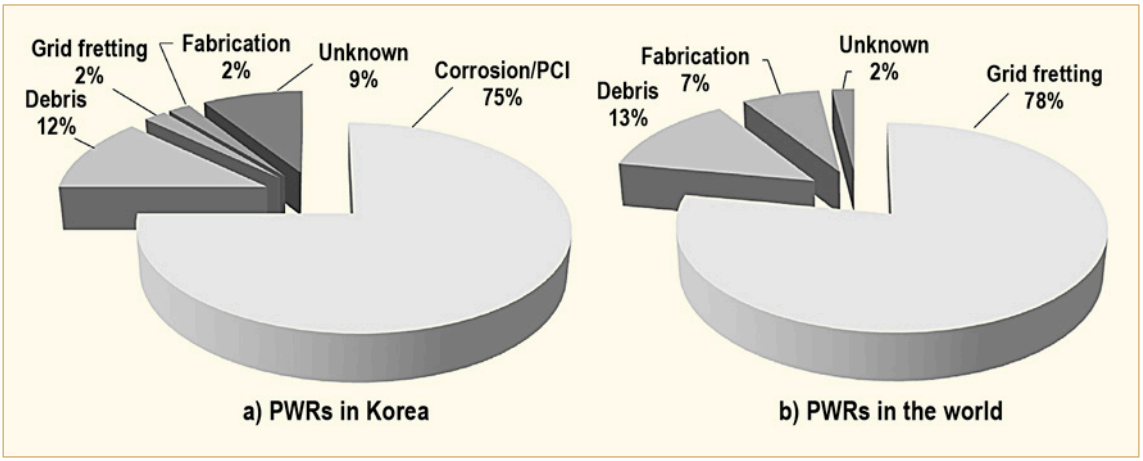

Figure 2-4: PWR fuel rod failure causes from the year 2002 to 2006 [Kim, 2013].

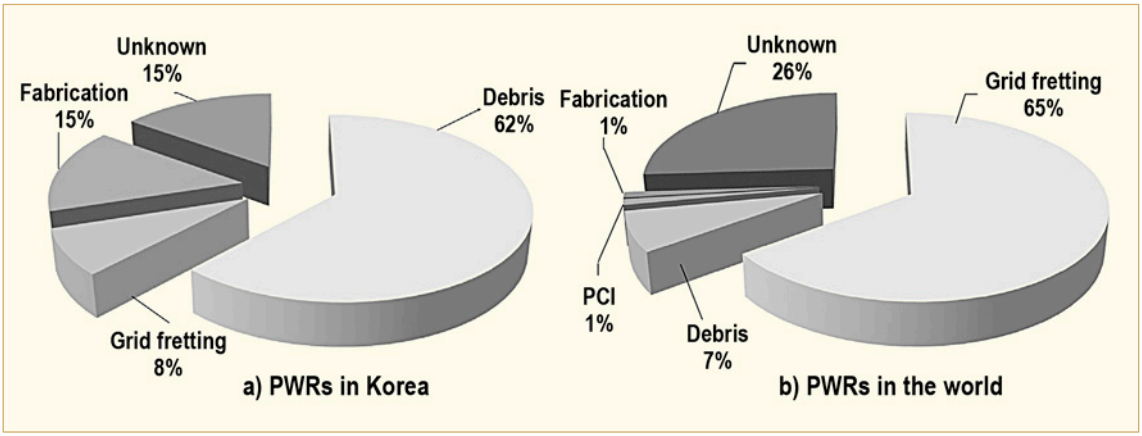

Figure 2-5: PWR fuel rod failure causes from the year 2007 to 2011 [Kim, 2013].

Table 2-2: Summary of major fuel failure causes, driving forces and countermeasures, after [Kim, 2013].

Failure type	Failure causes	Countermeasures
Grid-to-rod fretting (GTRF) wear	Excessive assembly vibration due to hydraulically unbalanced grid mixing vanes generating a rotational force on spacer grid assembly.	Develop a spacer grid assembly design having hydraulically balanced grid mixing vane patterns.
	Excessive grid strap vibration due to hydraulically unbalanced grid strap geometry.	Develop a spacer grid strap design having hydraulically balanced grid strap geometry such as thickness, length, window.
	Excessive fuel rod vibration due to untolerable grid-to-rod gap against grid-to-rod fretting wear.	Develop a spacer grid design with a large grid-to-rod contact area and in addition spacer grid spring with an optimized spring stiffness.
Debris-induced fretting wear	Foreign particles in the reactor cores such as wires, bolts, metal chips, etc.	Develop a debris-filtering device curved flow paths or smaller flow holes.
Excessive cladding corrosion	Accelerated corrosion of claddings above about 46 MWD/kgU or at hot spot location.	Develop advanced Zr cladding materials or use existing ones. Use lower peaking factors.
Pellet-to-Clad Interaction (PCI)	Excessive local cladding tensile hoop stress due to a power ramp during reactor start-up and power changes.	Optimize power operation guidelines, e.g., reduction of power ramp rate during reactor start-up, use of corrosion-resistant advanced zirconium alloys, etc.
Fuel assembly bowing	Excessive fuel assembly bowing due to weak grid thimble tube strength and excessive irradiation-induced growth of guide thimble and spacer grid materials.	Develop high-strength and irradiation growth-resistant guide thimble tubes as well as irradiation growth-resistant spacer grid materials.
		ANT International, 2013

The advanced fuel development and verification processes includes concept designs and screen tests, preliminary designs and scoping tests phase, detail designs and out-of-pile verification tests phase, and in-reactor verification tests (Figure 2-6 and Figure 2-7).

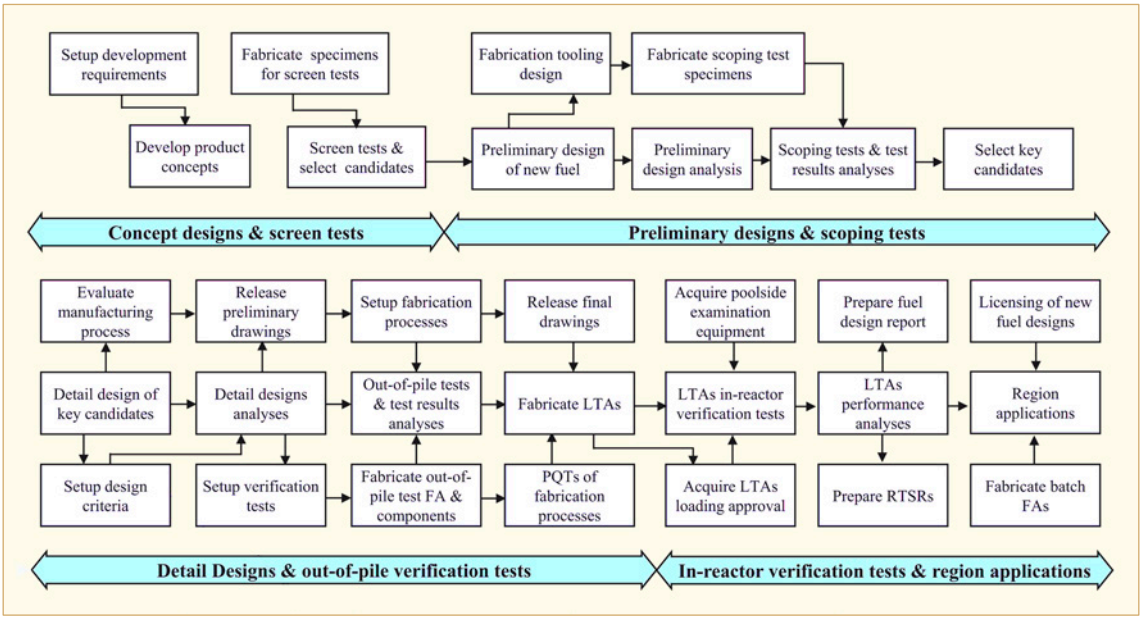

Figure 2-6: Development and verification processes of advanced fuel designs [Kim, 2013].

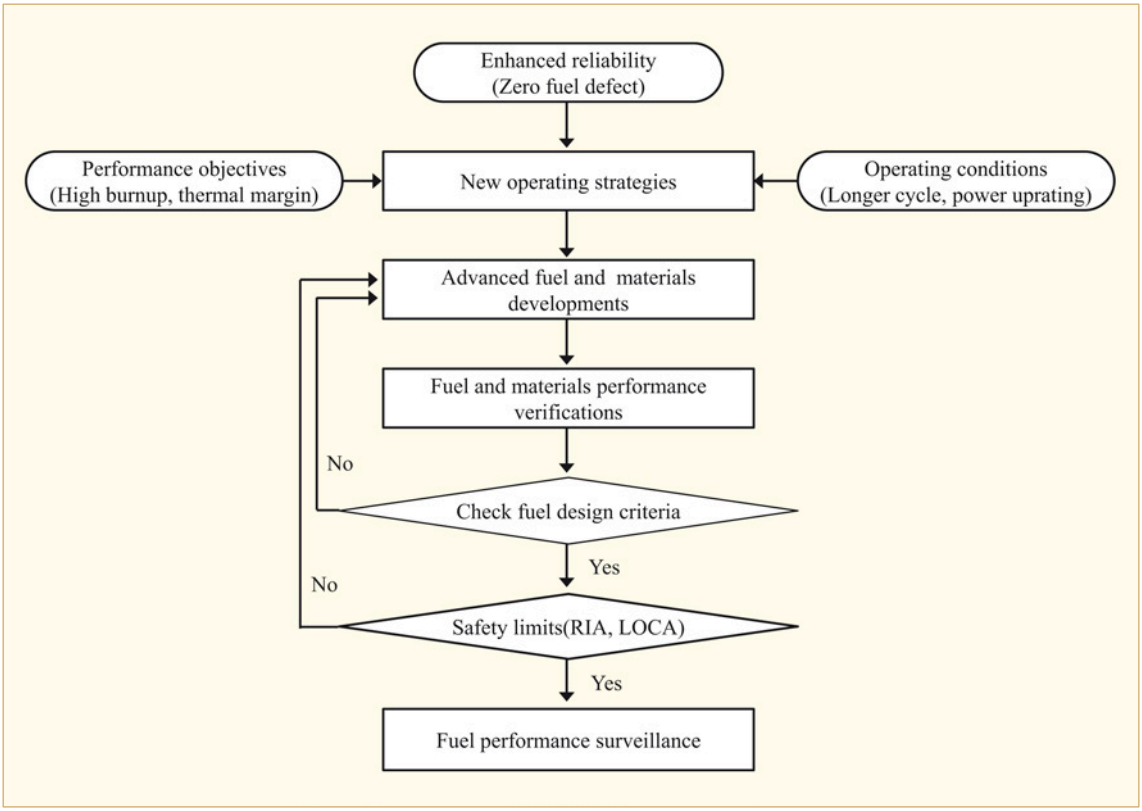

Figure 2-7: Overall advanced fuels and cladding materials development procedures.

Figure 2-8 gives an overview of verifications for new Zr alloy materials, including out-of-reactor, test reactor and tests in commercial reactors. *However, it is important to keep in mind that out-of-reactor tests often gives results that do not correlate with in-reactor performance – corrosion tests are an excellent example. The reason for the different material response out-of-reactor and in-reactor is that the mechanisms are often different in these two environment. Irradiation in test reactors are very expensive and costs so much money that often the tests cannot be carried out long enough to capture any material issues that may occur after longer irradiation times.*

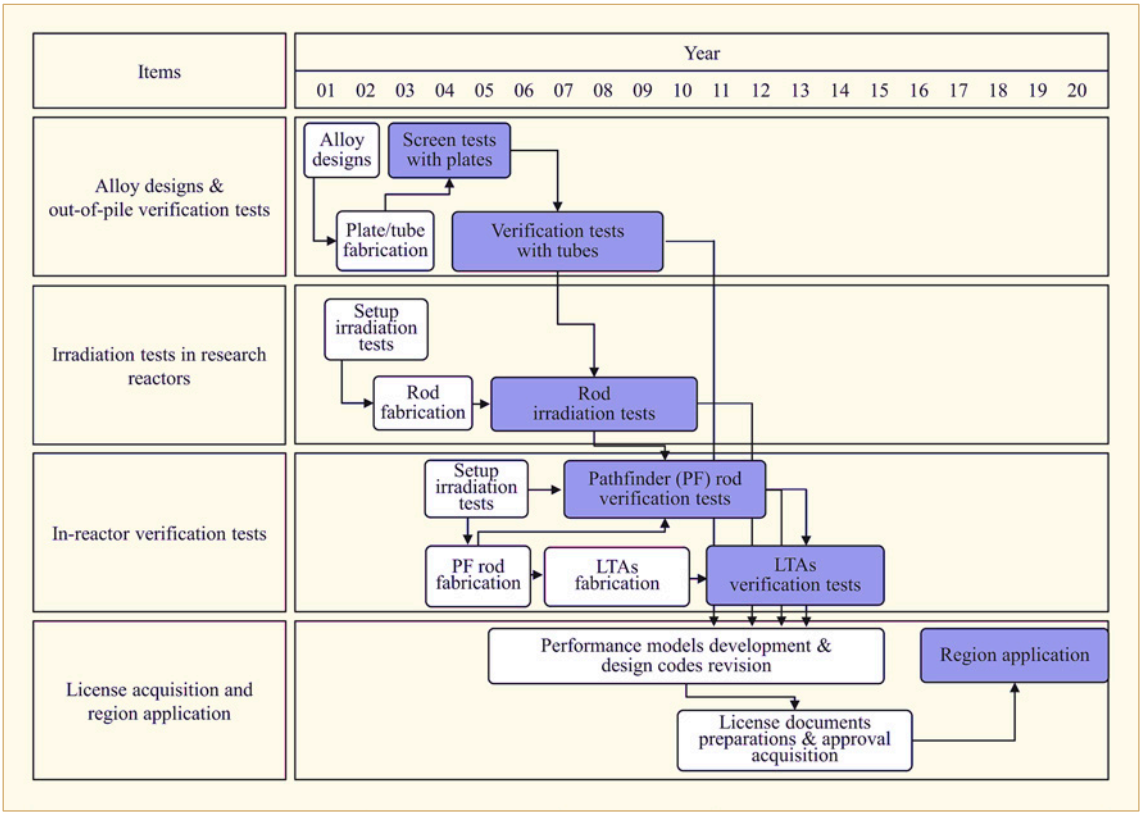

Figure 2-8: Development and verification processes of advanced fuel cladding materials [Kim, 2013].

The evolution of different 17 × 17 W-NSSS and 16 × 16 CE-NSSS PWR designs are specifically shown Figure 2-9 and Figure 2-10 (Table 2-3 and Table 2-4). Korea Nuclear Fuel (KNF) used to import fuels (i.e., Vantage-5H, RFA, STD and Guardian) from WEC before KNF verified their own advanced fuel designs. ACE7 and PLUS7 have been jointly developed by KNF and WEC. HIPER is being solely developed by KNF.

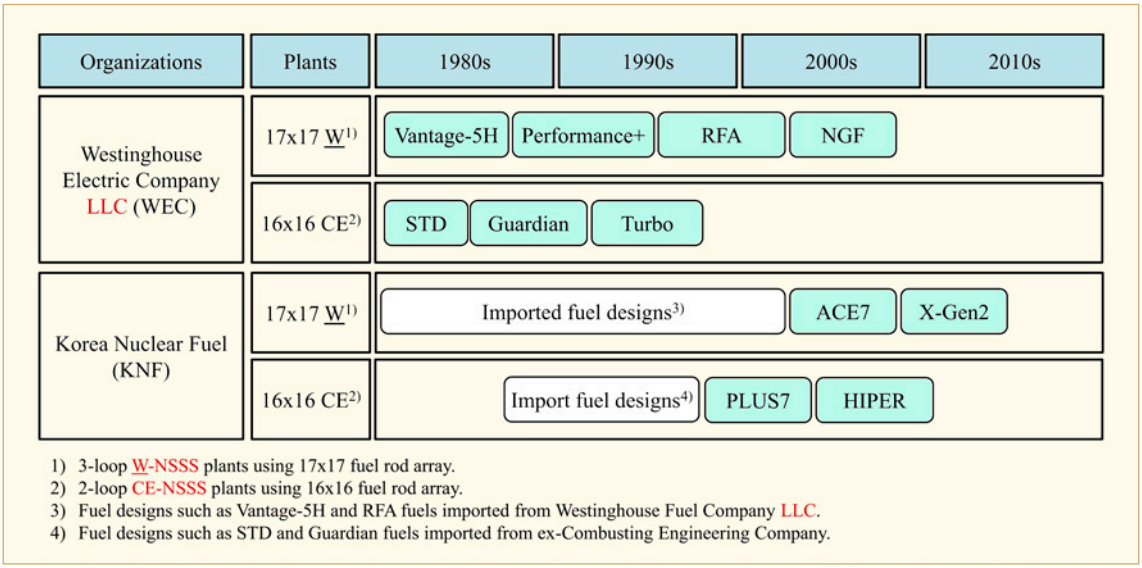

Figure 2-9: Histories of advanced PWR fuels developed by WEC LLC and KNF [Kim, 2013].

Table 2-3: Design features of advanced nuclear fuels for 17x17 W-NSSS plants, after [Kim, 2013].

Key data	**Imported fuels for PWRs in Korea**			**KNF's advanced fuel**
	Vantage-5H	**Performance+**	**Robust Fuel Assembly (RFA)**	**Next generation fuel (ACE7)**
Start of region application	1987	1992	1998	In-reactor verification completed
Discharged batch average burnup (MWD/MTU)	~45 000	~50 000	~50 000	~55 000
Overpower margin against PWR fuel without mixing vane (%)	~10	~10	~15	~25
Fuel rod diameter (mm)	9.50	9.50	9.50	9.50
Cladding materials	Zry-4 or ZIRLO	ZIRLO	ZIRLO	Opt-ZIRLO
Mid-spacer grid with mixing vanes	Yes	Yes	Yes	Yes
Number of spacer grid assemblies	8	8	8	8
Number of intermediate flow mixers	3	3	3	5
Spacer grid spring shape	Diagonal	Diagonal	Diagonal	Vertical
Spacer grid materials	Zry-4/Inconel	Zry-4/Inconel	ZIRLO/Inconel	Zry-4/Inconel
Guide thimble tube	Thin G/T and dashpot design	Thin G/T and dashpot design	Thick G/T	Tube-in-tube G/T
Debris filter design	Small flow-hole bottom nozzle	Small flow-hole bottom nozzle + protective grid	Small flow-hole bottom nozzle + protective grid	Small flow-hole bottom nozzle + protective grid
				ANT International, 2013

Table 2-4: Design features of advanced nuclear fuels for 16× 16 CE-NSSS plants, after [Kim, 2013].

Key data	Imported fuels for PWRs in Korea		KNF's advanced fuels	
	STD	Guardian	PLUS7	HIPER
Year of region application	1994	2001	2006	~2016
Discharged batch average burnup (MWD/MTU)	~45 000	~45 000	~55 000	~65 000
Overpower margin against PWR fuel without mixing vane (%)	0	0	~10	~15
Fuel rod diameter (mm)	9.70	9.70	9.50	9.50
Cladding materials	Zry-4	Zry-4/ZIRLO	ZIRLO	ZIRLO/HANA
Mid-spacer grid with mixing vanes	No	No	Yes	Yes
Number of spacer grid assemblies	11	11	12	11
Number of intermediate flow mixers	0	0	0	2
Spacer grid spring shape	Horizontal & leaf	Horizontal & leaf	Horizontal & conformal	Vertical
Spacer grid materials	Zry-4/Inconel	Zry-4/Inconel	ZIRLO/Inconel	HANA/Inconel
Guide thimble tube	Thick G/T	Thick G/T	Thick G/T	Thick G/T
Debris filter design	None	Standard flow-hole bottom nozzle + debris filter grid	Small flow-hole bottom nozzle + debris filter grid	Standard flow-hole bottom nozzle + debris filter grid
				ANT International, 2013

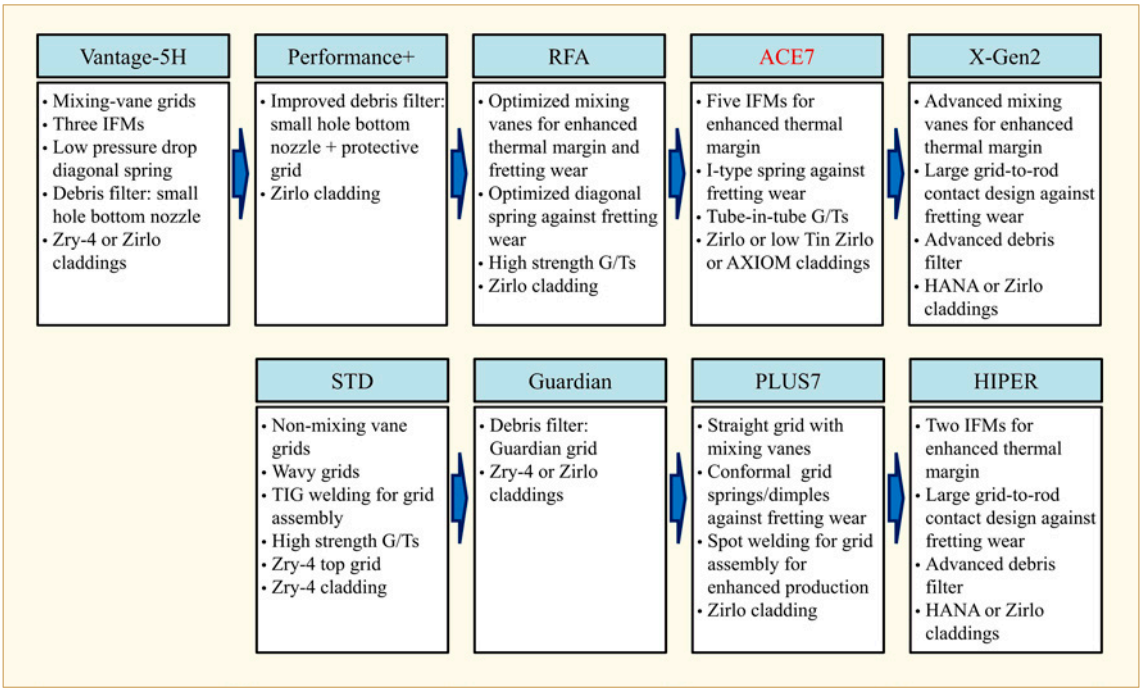

Figure 2-10: Evolutionary changes in design features of advanced PWR fuels [Kim, 2013].

Figure 2-11 and Figure 2-12 shows the up-to-date GTRF-resistant grid designs and their improved performance. Figure 2-13 provides information about 4 debris catcher designs either of a wavy flow-path type or a reduced flow-hole type while Table 2-5 summarizes their performance based on the debris filtering tests performed in this study by [Kim, 2013].

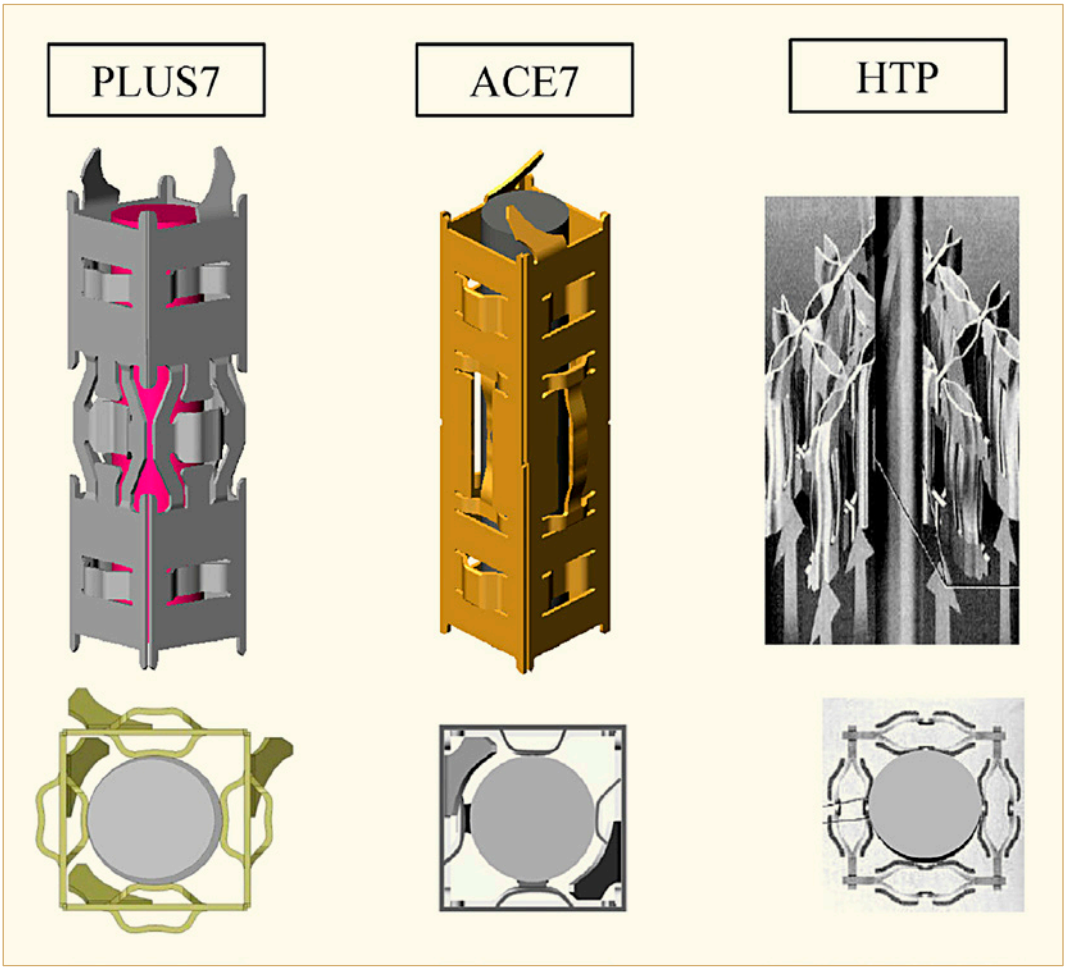

Figure 2-11: Up-to-date GTRF-resistant spacer grid designs [Kim, 2013].

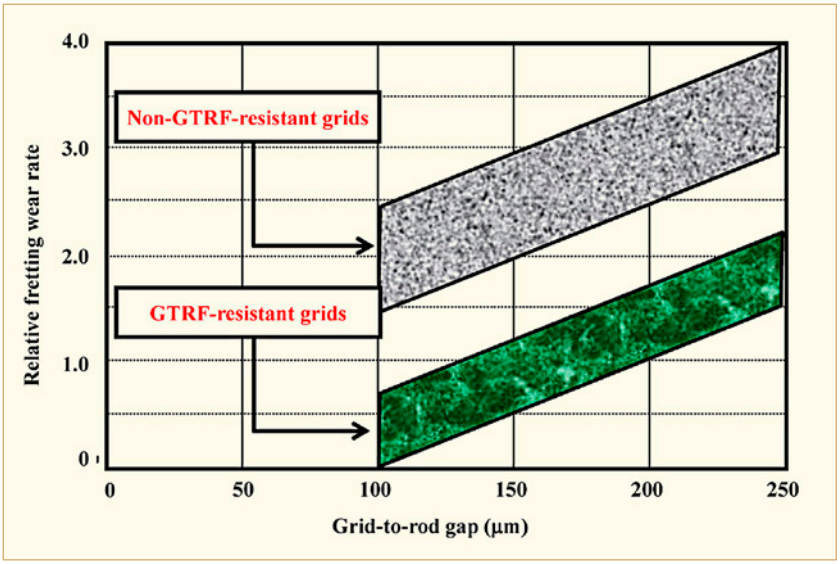

Figure 2-12: Enhanced grid-to-rod fretting wear rates of the PLUS7 grid against standard grids [Kim, 2013].

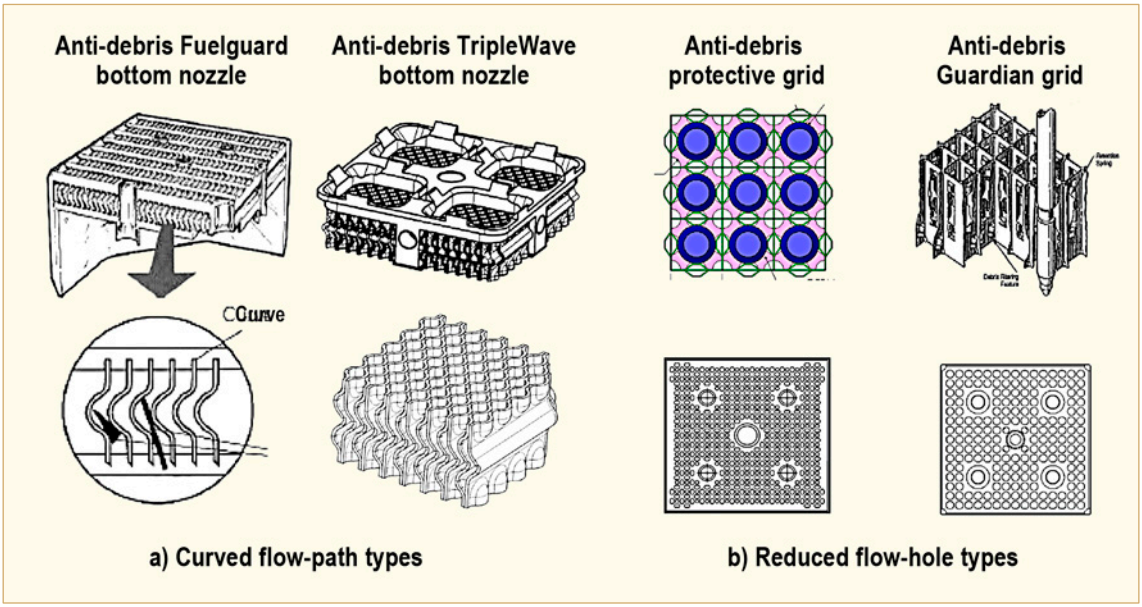

Figure 2-13: Up-to-date debris filter designs [Kim, 2013].

Table 2-5: Evolution of debris filtering efficiency of advanced fuel designs, after [Kim, 2013].

Locations	Debris filtering efficiency (%)		
	STD[a]	PLUS7[b]	Guardian[c]
Bottom nozzle	26.3	59.3	26.3
Debris filter grid	-	31.9	70.0
Total	**26.3**	**91.2**	**96.3**

[a] STD fuel having a standard large flow-hole bottom nozzle.
[b] PLUS7 fuel having a small flow-hole bottom nozzle and protective grid.
[c] Guardian fuel having a standard large flow-hole bottom nozzle and Guardian grid.

ANT International, 2013

To reduce the tendency for fuel assembly bowing which could potentially result in incomplete control rod insertion (IRI), the stiffness of the Guide Tubes have been increased (Figure 2-14).

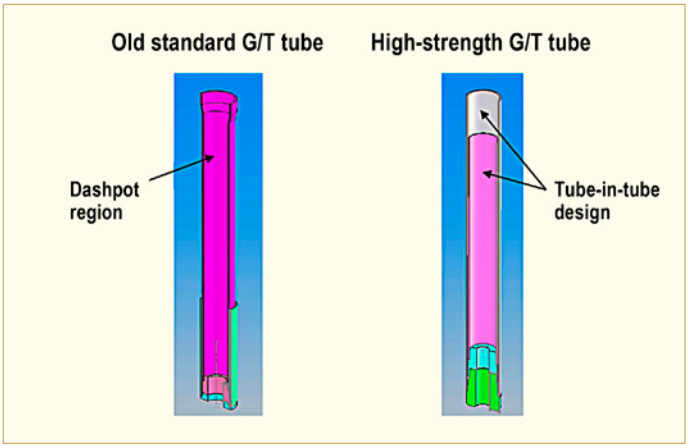

Figure 2-14: Comparison of the G/T dashpot design and the tube-in-tube design [Kim, 2013].

Table 2-6, Figure 2-15 and Figure 2-16 gives an overview of the HANA 4 and 6 new cladding material in comparison to other advanced PWR alloys developed by non-Korean fuel vendors.

Table 2-6: Summary of PWR cladding tube compositions, after [Kim, 2013].

Cladding materials		Chemical element composition (w/o)						
		Zr	Nb	Sn	Fe	Cr	Ni	Cu
	Zry-4	Balance	-	1.5	0.2	0.1	-	-
USA	ZIRLO Opt-ZIRLO X5A	Balance Balance Balance	1.0 1.0 0.3	1.0 0.7 0.5	0.1 0.1 0.35	- - 0.25	- - -	- - -
France	M5	Balance	1.0	-	-	-	-	-
Japan	NDA MDA	Balance Balance	1.0 0.5	1.0 0.8	0.27 0.2	0.16 0.1	0.01 -	- -
Russia	E110 E635	Balance Balance	1.0 1.0	- 1.3	- 0.4	- -	- -	- -
Korea	HANA4 HANA6	Balance Balance	1.5 1.1	0.4 -	0.2 -	0.1 -	- -	- 0.05

ANT International, 2013

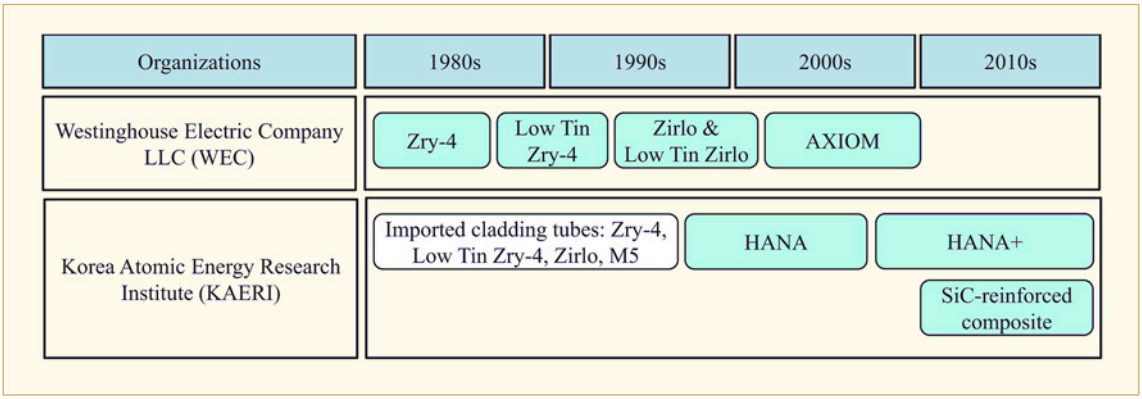

Figure 2-15: Histories of advanced PWR cladding materials developed in the USA. and Korea [Kim, 2013].

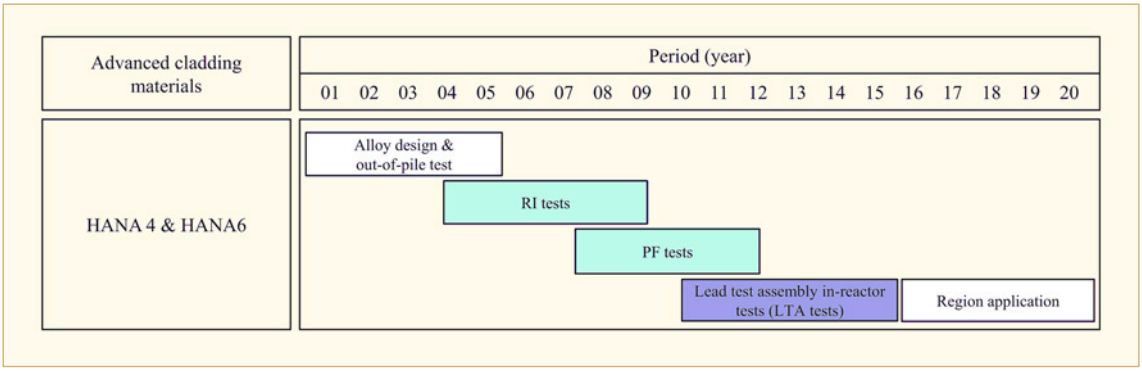

Figure 2-16: Stepwise developments of HANA cladding materials [Kim, 2013].

2.4.2 European fuel group (ENUSA and Westinghouse)

The paper by [Chapin et al, 2013] describes the EFG[1] fuel designs used in the Ringhals PWRs and the operating performance of the designs. The fuel cladding material is Optimized ZIRLO with ZIRLO used for the structural material. Plant-specific analyses were performed for the Ringhals Units to meet the requirements for qualification and licensing of the EFG fuel and to demonstrate compatibility with fuel designs operating in transition cores.

Four New Generation Fuel (NGF) Lead Fuel Assemblies (LFA) were manufactured and delivered to Ringhals 4 in the spring of 2013 and the assemblies will be irradiated for four or possibly five annual cycles. The main features of the 17x17 NGF product in comparison with the Westinghouse 17x17 Robust Fuel Assembly (RFA) design are:

- The Low Tin ZIRLO skeleton structure to increase dimensional stability and
- New NGF mid-grid designs:
  - Larger cladding/spring contact area with the I-spring provides larger Grid to rod fretting (GTRF) margins.
  - Improved flow mixing and thermal performance relative to the RFA mid-grids,
  - Added features to improve grid-to-grid interactions during assembly handling.
- 5 NGF Intermediate Flow Mixer (IFM) grids compared to 3 IFMs in the RFA product:
  - Improve the thermal performance which enables increased DNB and CIPS margins as well as improved loading pattern options.
  - Stiffens both the fuel rods and fuel assembly thus reducing fuel rod/assembly bowing.

Poolside examinations will be performed to monitor the performance of the 4 LFAs.

2.5 New advanced fuel materials

2.5.1 Fuel

IAEA published a report which summarizes the current status of nuclear fuel manufacturing technology for both power and research reactors, and to highlight the trends that are emerging for advanced fuels [IAEA-TECDOC-1686, 2012]. The report covers manufacturing of the following fuel types:

- Uranium and mixed uranium plutonium mixed oxide fuels
- Thoria and thoria based fuels
- Mixed carbide and nitride fuels
- Metallic fuels
- Fuels for research reactors

[1] The European Fuel Group (EFG) is an alliance between Westinghouse and ENUSA which supplies fuel designs and technology to European PWR plants.

2.5.2 Zr alloys

[Savchenko et al, 2011] presented a novel class of ternary or quaternary eutectic zirconium alloys having relatively low melting point i.e. from 690 to 860°C in comparison with pure zirconium. The new alloys are intended for use as a matrix of a dispersion high uranium content fuel (CERMET and METMET) particularly for thermal reactors (Table 2-7).

Table 2-7: Alloy compositions, melting and impregnation temperatures (T). Other elements: Nb, Cu, Gd, Mo, Al, Si, B, U, Pu, after [Savchenko et al, 2011].

Group number	Alloy composition (wt%)					Melting T (K)	Impregnation T (K)
	Zr	Ti	Fe	Cu	Be		
1	Base	-	6-12	6-12	-	1123-1133	1173-1183
2	Base	-	4-8		2-3	1053-1083	1123-1143
3	Base	5-10	8-14	8-14	-	1083-1093	1153-1173
4	Base	5-20	4-7	1-3	1.5-2.5	963-993	1053-1083

ANT International, 2013

The main second phase is the body centred tetragonal $Zr_2(Fe,X)$ phase in the α-Zr alloy matrix [Savchenko et al, 2011]. In these alloys, X is elements Cu, Be, Ni, Nb, Al, Si (see Figure 2-17). Depending on the compositions of the alloys other second phases are, Zr_2Cu and $ZrBe_2$. Since zirconium forms the base of the matrix alloys, these alloys are compatible with the high uranium content fuel both upon fabricating fuel elements and after long-term isothermal anneals of fuel composition at 1023 K for 6000 h (Figure 2-18).

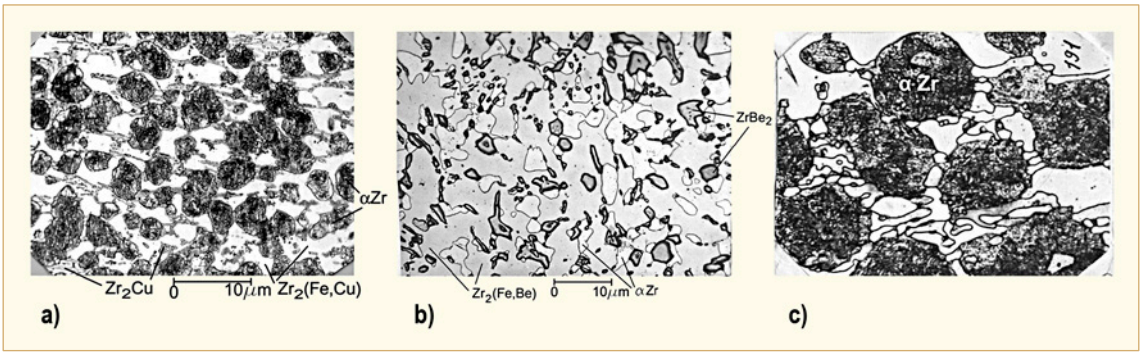

Figure 2-17: Microstructures of alloys for the systems: (a) Zr-Fe-Cu, (b) Zr-Fe-Be, (c) hypoeutectic Zr-Fe-Cu [Savchenko et al, 2011].

3 Microstructure

A limited amount of information was published on this topic during the last 18 months.

4 Mechanical properties

The relevant information is published in the associated ZIRAT18/IZNA13 Special Topic Reports on Mechanical Testing.

5 Dimensional stability (Ron Adamson)

5.1 Introduction

Several papers from the 17th International Symposium-Zirconium in the Nuclear Industry in February 2013 (Hyderabad, India) provide new insights into creep and growth of zirconium alloys. Unfortunately, most papers have not yet cleared peer-review. This ZIRAT/IZNA AR review relies on the oral presentations and pre-publication versions of the work.

An overall capsule review of the meeting in the 2013 ZIRAT17 meetings is presented here:

Brief review:

- About 150 attendees:
  - 13 countries
  - 20 countries
- Numbers of authors per paper:
  - Ave./median – 6-7
  - Min. 3 – max.17
- Number of collaborating organizations per pater:
  - Ave. 3
  - Median 2
- All presentations will be on the ASTM website
- Symposium book out in 12-18 months:
  - No longer will papers be published on on-line journal
- Next meeting – May 15-19, 2016, Hilton Head Westin, South Carolina

Sessions:

- Basic metallurgy (6):
  - Movement of H and alloying elements in heterogeneous materials based on thermodynamics
  - Effects of Fe in M5
- Fabrication (6):
  - Mainly Zr2.5Nb
  - Protective coatings on Zr-alloys (for high temperature applications)
- Corrosion and hydriding (6):
  - Many advanced techniques and exams of oxides:
    - Atom probe, STEM, synchrotron, ion irradiation, SIMS, cold-neutron-prompt-gamma-activation
  - Some progress is occurring

- In-pile performance (6):
  - Variations in Zr-Sn-Nb-Fe compositions:
    - E635 seems to have best corrosion/hydriding (caution-duty and water chemistry): E635<op ZIRLO, <ZIRLO
    - ZIRLO shows acceleration of corrosion and HPUF near 65 GWd/mt
    - ZIRLOS have Oxide Surface Peeling (OSP) at high BU
  - Zr2.5Nb creep behaviour
- Irradiation and H effects:
  - Very good session
  - Several excellent irradiation growth papers
  - 2 papers on 1) experimental and 2) first principle modelling effects of H on <c> loop formation
- High temperature transient (6):
  - 30 microns pre-film oxide improves performance
  - Nitrogen atmosphere degrades performance
  - E110G much better than E110:
    - Si up, Fe up, Hf down
    - No information on surface condition
- Degradation and failure mechanisms:
  - In-situ synchrotron study of hydride orientation
  - Li in BWR oxide detrimental to corrosion failures
  - H does not affect DHC velocity
- Posters (31):
  - Some clarification of H(delta V) expansion
  - Fe congregates at g.b. and beta Nb surfaces
  - Fatigue etc.

Kroll medals:

- Mr. Jack Kearns – Bettis Atomic Power Laboratory, USA
- Dr. Srikumar Banerjee – Department of Atomic Energy, India:
  - Metallurgy and fabrication of Zr alloys

5.2 Analytical/Computational papers

The paper by [Golubov et al, 2013] takes a mathematical/analytical/first-principle approach to describing irradiation growth, starting with the creation of interstitials (SIAs), vacancies (V) and SIA clusters (SIACs, for use here) during the initial neutron damage event. Key to the analysis are:

- V diffusion is isotropic in the Zr lattice. *This is widely accepted in the literature.*
- SIA diffusion is isotropic in the Zr lattice. *This is not a common assumption in the literature.*
- SIAC diffusion is anisotropic, favouring motion on the basal planes in <a> directions. *Not much literature exists on this point, except by recent work by Golubov and his colleagues.*
- There is a non-uniform distribution of a-type dislocations in the lattice. *Again, not much in the Zr literature, but a reasonable assumption.*
- SIACs (which have a Burgers vector) interact with a-type dislocations and the interaction is different when a-dislocations have different (6 different) directions of their Burgers vectors.
- The growth strain and strain rate depend not on the magnitude of the densities of a- and c-dislocations (<a> and <c>- component dislocation loops), but on the ratios of a- and c-dislocation densities, a/c. A fallout of this is that growth strain rate decreases as the ratio of a-density to c-density increases.

The paper does not deal with the initiation of either <a>-loops or <c>-loops, but uses experimental observation to state their existence and character.

The paper uses Zr single crystal growth data by [Carpenter et al, 1988] as a benchmark (Figure 5-1), and attempts to predict all common growth observations, such as the shape of the curves in Figure 5-2. The maximum growth strain rate is predicted to be between 1 – 10 x 10^{-3} per dpa (or about 1.7x10^{16} per n/cm^2 (E>1MeV), presumably for single crystal Zr. That growth rate compares to about 0.6x10^{-3}/dpa calculated from the data of [Mahmood et al, 2000]. *Considering variables such as temperature, texture, data scatter, computational uncertainties, etc. the comparison is surprisingly good.*

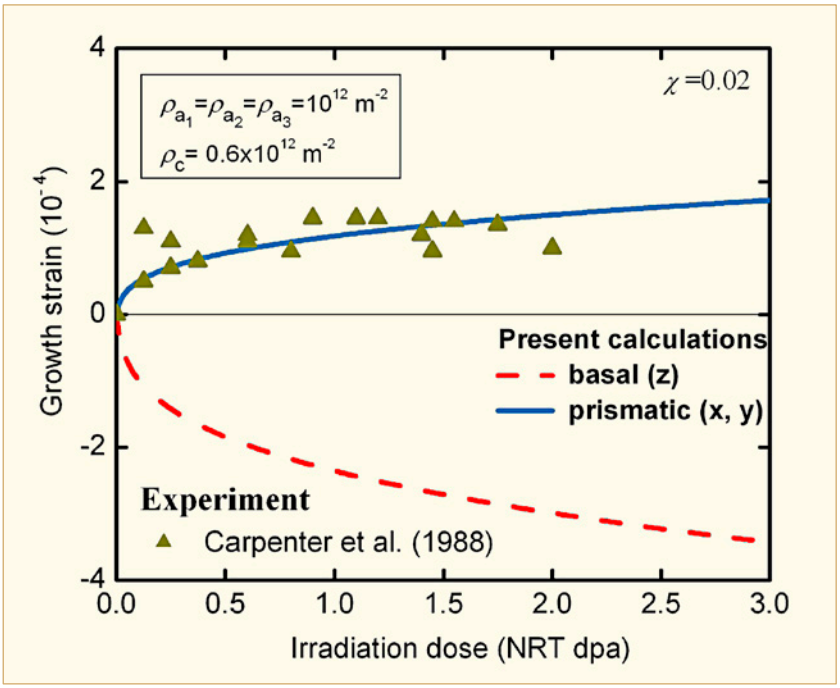

Figure 5-1: Best-fit calculations as compared to experimental data of [Carpenter et al, 1988], [Golubov et al, 2013].

6 Corrosion and hydriding (Friedrich Garzarolli)

6.1 Mechanistic aspects for corrosion and hydriding of Zr alloys corrosion

6.1.1 Oxidation mechanism

6.1.1.1 Overview on the state of knowledge

An extensive review on the mechanism of corrosion and hydrogen pickup was given in the ZIRAT12/IZNA7 STR on Corrosion Mechanism and in the ZIRAT16/IZNA11 Annual Report Section 6.1. Here an update of the corrosion mechanism is given considering especially the recent reported literature.

Corrosion kinetics

Zirconium and its alloys are highly reactive with oxygen-containing environments and become covered by an oxide film. The oxide layer growing rate increases exponentially with temperature.

The corrosion kinetics in pressurized water exhibits initially a power law dependence on time with an exponent of about 3, what means that the rate of oxidation gets progressively slower. However, when an oxide thickness of 1.5-3 μm is reached a transition occurs and the oxidation rate returns to much faster growth. The initial process apparently repeats itself thereafter and this event re-occurs at fairly regular intervals, leading to a growth kinetics which in average appears to be essentially linear.

At certain alloy contents, temperature range, system pressures, impurity level, and irradiation the corrosion rate my significantly accelerate after a short initial period.

Oxygen in the corrosion environment has not much effect on out reactor corrosion [Garzarolli et al, 1989] but increases corrosion of ZrNb alloys significantly. In high pressure (>70 bar) steam at 420-550°C a localized corrosion, the so called nodular corrosion may appear in sensitive Zry-2/4 lots.

The effect of irradiation depends on the oxygen content of the coolant (Figure 6-1). In oxygenated coolant (BWR) irradiation increases corrosion especially at the early beginning. Furthermore, nodular corrosion may start in reactor after 10 to 100 days and shadow corrosion after a few days if a SS or Inconel component is close or in contact [Garzarolli & Sell, 2006]. At high burnups, when the SPP are mostly dissolved by irradiation, uniform corrosion may accelerate.

In the oxygen free hydrogenated coolant in PWR normally only uniform corrosion appears, that is in case of Zry-4 significantly enhanced in reactor compared to out reactor above a certain oxide layer thickness (~5 μm). The corrosion of PWR fuel rods is governed by the temperature at the metal oxide interface. The temperature increase over oxide, which increases with increasing oxide thickness and heat flux, can therefore accelerate the corrosion rate in PWR [Garzarolli et al, 2001].

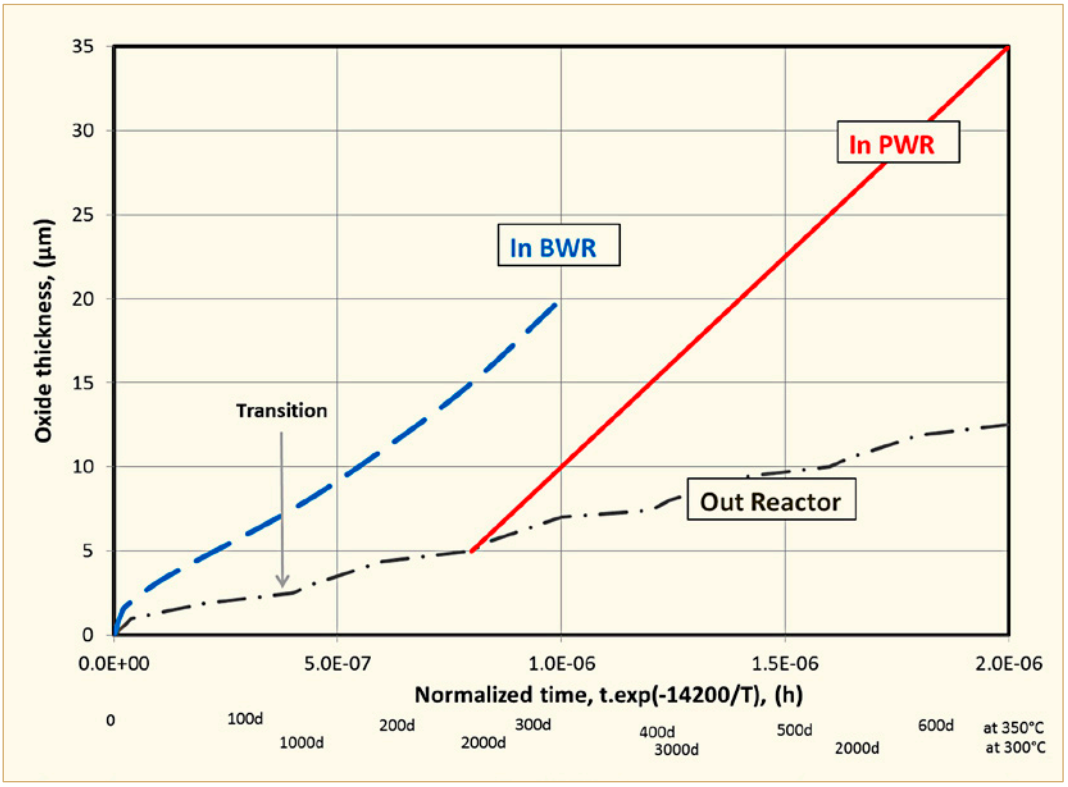

Figure 6-1: Effect of irradiation on corrosion behaviour in PWR and BWR according own analysis.

Electrochemical aspects

From electrochemical stand point the corrosion process of Zr alloys is as shown in Figure 6-2 governed by:

- The **anodic reaction** at the M/O interface, where O-ions from the oxide layer (O^{2-}) react with metallic Zr and form ZrO_{2-x}, electrons (e-), and O-ion-vacancies in the oxide layer (VO^{2+})
- and the cathodic reaction at the oxide-water interface where O-ion-vacancies (VO^{2+}) and electrons (e-) that diffused out from the metal oxide interface react with H_2O and release H atoms respectively H^+ and OH^- ions

The reaction rate is governed by (1st) the thickness of the protective oxide layer, (2nd) the O-ion-vacancy (VO^{2+}) diffusion rate, and/or (3rd) the resistance against electron (e-) migration.

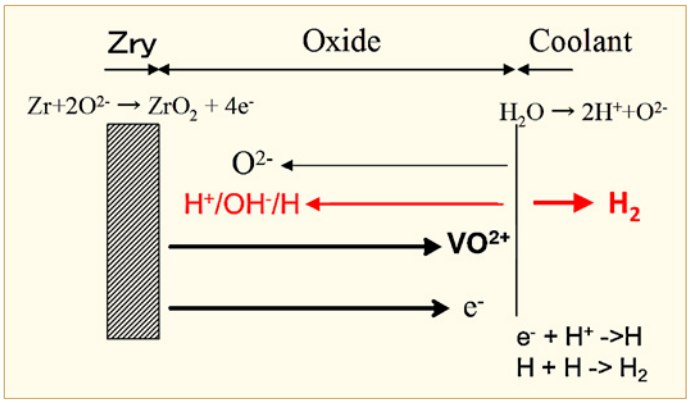

Figure 6-2: The electrochemical process of Zr-alloy corrosion.

Oxide layer structure

The oxide layer on Zr alloys has generally an outer porous and an inner dense part. Impedance measurements in H_2SO_4 at RT as well as in-situ in autoclave under corrosion at e.g. 350°C have shown that in case of uniform corrosion up to an oxide thickness of about 2-4 µm (transition) a mayor part of the oxide layer is dense. After the transition an inner layer of 0.3 and 3 µm (barrier layer) remains dense, whereas the rest becomes porous (Figure 6-3). In water with 70 ppm LiOH, which accelerates corrosion, the dense part of the oxide layer was estimated by the Li profile in the oxide. Here the transition occurs somewhat earlier and the dense interlayer is reduced to a lower value, to ~0.2 µm. In case of the very fast nodular corrosion a significant fraction of the oxide layer becomes porous at >0.1-0.3 µm and the barrier layer becomes very low, only about 0.03 µm.

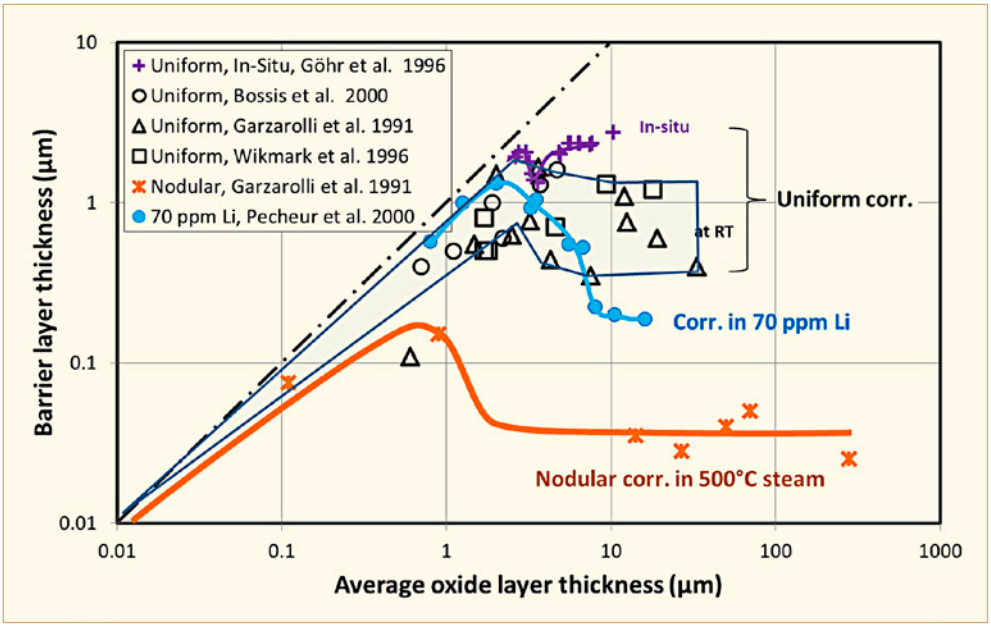

Figure 6-3: Thickness of the dense barrier layer in oxide layers formed out reactor vs. total oxide thickness, exhibiting a decrease at the rate transition.

Besides the stable monoclinic ZrO_2, tetragonal, cubic, and amorphous phases were detected especially at the oxide interface, e.g. [Zhou et al. 2008], which are stabilized by stresses respectively their lower surface energy, as will be discussed more detailed later on.

The studies on the grain structure within the oxide layer have generally shown, that the grain morphology in the oxide layers consists of columnar and equiaxed grains. Most studies reported that the outermost layer, which has formed at first in the pre-transition range, consists by primarily equiaxed grains e.g. [Garzarolli et al, 1991]. The columnar grains have different widths/lengths ratios depending on the alloy. They are most perfect developed in oxides grown on most corrosion resistant alloys, and are rather short and contain a high fraction of equiaxed grains in uniform oxide layers grown on fast corroding materials, e.g. Zry-4 with fine SPP, e.g. [Garzarolli et al, 1991] and [Anada et al, 1996], or in environments that lead to high corrosion e.g. [Pêcheur et al, 1996]. The columnar grains extend sometimes up to the oxide/metal interface, e.g. in the Zr–2.5Nb alloy, but in other alloys (ZIRLO, NDA and Zircaloy-4) a higher percentage of equiaxed grains is usually seen at the oxide/metal interface. The size of the columnar grains, estimated from the width of diffraction peaks is about 20 nm for Zry-4 and ZIRLO, and somewhat larger (28 nm) for Zr2.5Nb compared to that of the equiaxed tetragonal grains about 8 nm. The values estimated with TEM are 10-80% higher [Motta et al, 2005]. The width of the columnar oxide grain increases further with increasing distance from the M/O interface.

7 Primary failure and secondary degradation – open literature data (Peter Rudling)

The open literature data are provided in the following sections.

7.1 Introduction

7.1.1 Primary failures

During reactor operation, the FR may fail due to a primary cause such as fretting, PCI manufacturing defects, corrosion, etc. (Table 7-1).

Table 7-1: Primary failure causes for LWR fuel during normal operation and Anticipated Operational Occurrences (AOO).

Primary failure cause	Short description
Excessive corrosion	An accelerated corrosion process results in cladding perforation. This corrosion acceleration can be generated by e.g., CRUD deposition (CILC[20]), Enhanced Spacer Shadow Corrosion, (ESSC),[21] (in BWRs), dry-out due to excessive FR bowing.
Manufacturing defects	Non-through-wall cracks in the fuel cladding developed during the cladding manufacturing process. Defects in bottom and/or top end plug welds. Primary hydriding due to moisture in fuel pellets and or contamination of clad inner surface by moister or organics. Too large a gap between the FR and the spacer grid supports (poor spacer grid manufacturing process) leading to excessive vibrations in PWR fuel causing fretting failures. Chipped pellets may result in PCI failures both in liner and non-liner fuel.
PCI	PCI—an iodine assisted SCC phenomenon that may result in fuel failures during rapid power increases in a FR. There are three components that must occur simultaneously to induce PCI and they are: 1) tensile stresses—induced by the power ramp, 2) access to freshly released iodine-occurs during the power ramp, provided that the fuel pellet temperature becomes large enough and 3) a sensitised material—Zircaloy is normally sensitive enough for iodine stress-corrosion cracking even in an unirradiated state.
Cladding collapse	This failure mechanism occurred due to pellet densification. This failure mode has today been eliminated by fuel design changes and improved manufacturing control.
Fretting	This failure mode has occurred due to: Debris fretting in BWR and PWR. Grid-rod fretting - Excessive vibrations in the PWR FR causing fuel failures. This situation may occur for example due to different pressure drops in adjacent FAs causing cross-flow. Baffle jetting failures in PWRs - Related to unexpectedly high coolant cross-flows close to baffle joints.
	ANT International, 2012

[20] CILC – an accelerated form of corrosion that has historically resulted in a large number of failures in BWRs. Three parameters are involved in this corrosion phenomenon, namely: 1) Large Cu coolant concentrations as a result of e.g., aluminium brass condenser tubes, 2) Low initial fuel rod surface heat flux – occurs in Gd rods and 3) Fuel cladding that shows large initial corrosion rates- occurs in cladding with low resistance towards nodular corrosion.

[21] This corrosion phenomenon resulted in a few failed rods. The mechanism is not clear but seems to be related to galvanic corrosion. This corrosion type may occur on the fuel cladding in contact or adjacent to a dissimilar material such as Inconel. Thus, this accelerated type of corrosion occurred on the fuel cladding material at spacer locations (the spacer springs in alloy BWR fuel vendors fuel are made of Inconel). Water chemistry seems also to play a role if the fuel cladding material microstructure is such that the corrosion performance is poor. Specifically coolant chemistry with low Fe/(Ni-Zn) ratio seems to be aggressive (provided that the cladding material shows poor corrosion performance. A fuel cladding material with good corrosion resistance does not result in *ESSC*, even in aggressive water chemistry.

Table 7-2 and Table 7-3 provide key data for some of the most recent fuel-failure cases.

Table 7-2: Summary of previous PWR failure key events, see previous ZIRAT/IZNA-reports for details.

Nuclear unit	Type of primary failure	Comment
TMI-1, Cy 10, 1995	Nine high peaking FRs, Zry-4 Cladding, failed after 122 days of operation. CRUD/corrosion related failures.	All failed and degraded pins reportedly had Distinctive CRUD Pattern (DCP)[22]. High peaking factors, thermal-hydraulic conditions. Calculations indicated that no boiling should have occurred on the pins with DCP, although the pins with DCP were calculated to have a slightly higher temperature. Water chemistry (low pH at BOC, pH < 6.9, max LiOH 2.2 ppm). Some, AOA effect was found reaching a maximum in the middle of cycle 10. The source of the CRUD could not be determined. The CRUD sampling showed that the nickel-to iron ratio was in the range 1.25 to 16.7, which was reportedly somewhat lower than in previous investigations.
Seabrook, Cy 5, 1997	Five one-cycle ZIRLO rods failed. CRUD/corrosion related failures.	Longer cycle in transition to 24-month cycle. Possibly CRUD-induced overheating resulting in substantial nucleate boiling.
EdF data reported in 2009 [Thibault et al, 2009]	The main failure causes in the EdF plants are: GTRF wear, Clad manufacturing defects and, Excessive fuel assembly bowing (resulting in assemblies grids hanging-up during loading and unloading and IRI)	A significant number of fuel failures were related to the M5 fuel cladding in 1300 MWe and 1450 MWe units. The M5 FR failures were due to fabrication defects either related to the end plug girth or fill hole weld or defects in the fuel clad itself at grid levels (related to the pulling of the rods into the assembly structure). To resolve these manufacturing issues, AREVA has modified the welding techniques as well as the rod pulling procedure. It was observed that there were no GTRF failures in 2008 (in previous years there have always been some GTRF failures). The reasons for the great improvement is thought to be due to that both AREVA and Westinghouse have introduction reinforced FAs design (AFA3GLr – AREVA and RFA2-Westinghouse). Since the introduction of the AREVA AFA3G design in 1999, a decrease of the average core bow in EdF NPPs has been observed, especially on the 900 MW units, but not as fast as expected. The maximum values of bowing remain relatively high on the 1300 MW units, typically between 15 and 19 mm for a “S shape” bow. The Westinghouse RFA fuel design behaves in the same way with similar bowing range while HTP assembly deformations are twice less. Incomplete Rod Insertions (IRIs) due to bowing have been significantly reduced since the AFA3G FA’s design has been loaded in EdF NPPs and despite the increasing of the average discharge burnup of the FAs. In 2008, no anomaly of RCCA drop time was observed in EdF NPPs during the BOC tests. Concerning the EOC tests, no anomaly was observed in the 12 feet units whereas four RCCAs dropped without recoil in the 14 feet units. Three of them was AFA3G FAs (two “2nd cycle” FAs and one “4th cycle” FA) and one was the older design (AFA2G). The number of FAs damaged during handling operations has decreased in 2008 but remains significant. The damages concern only AFA 2G or 3G design and mainly the 14 feet units. It occurs during the unloading operations. The damages generally occur during a “three-sided box” extraction and result from grids’ hanging due to bowing and to a reduced gap between FAs following unexpected grid growth due to re-crystallized Zircaloy-4.
		ANT International, 2012

[22] This acronym implies that the fuel inspection revealed CRUD deposits on the fuel rod and that the deposits were uneven in the rod circumference.

Table 7-3: Summary of previous BWR failure key events, see previous ZIRAT/IZNA-reports for details.

Nuclear unit	Type of primary failure	Comment
KKL	1997, 1998	Excessive Shadow Corrosion on LK II Zry-2 Cladding under the Inconel x-750 grid springs. The oxide thickness was locally above 500 µm. The most notable cladding corrosion attacks were found on fuel that had experienced a fourth, fifth, or sixth operational cycle. Zn-injection. Low level of Fe in coolant.
River Bend	Cy 8, 1999	At least 12 GE First cycle FRs were failed. Heavy CRUD - The failures appeared in bundles with a significant iron CRUD deposition. The heavy deposits almost filled the gaps between the FRs. Some 700 pounds (320 kg) iron was estimated to have been input to the River Bend-1 RPV during cycle 8 (1998-1999). CRUD deposit thickness in the range 37–55 mils (940 – 1400 µm) was reported. Analysis of the CRUD showed that the major phases were hematite and spinel, reportedly magnetite or zinc ferrite. Significant amounts of copper, up to 15% were found in some cases. No NMCA. Zn-injection.
Vermont Yankee, 2001-2002	5 FRs failed due to CRUD corrosion.	A total of 5 failed GE rods in 4 bundles were removed from the core at Vermont Yankee in a mid-cycle outage in May 2002, along with 40 other bundles deemed most at risk of failure due to being similar to the leakers in terms of duty, exposure, and tubing material.
Browns Ferry 2, Cy 12, 2001-2003	63 FAs failed due to localised massive hydriding	Affected fuel was GE13B claddings that failed in their second cycle with burnups of 29-30 MWd/kgU. Bundles that failed tended to be leading for the reload batch, indicating some impact of duty on tendency for failures. HWC started in BOC Cy 11 and NMCA at EOC 11 was implemented (3/01), Depleted Zinc Oxide (DZO) started in 1997 at 3 to 5 ppb. Maximum oxide thickness both in lower and upper part of the failed rods. Maximum CRUD deposition towards the bottom of the rods. BF2 changed out their condenser tubes to Ti-tubes 8-10 years ago.
Browns Ferry 3, Cy 11, 2002-2004	3 FAs failed due to localised massive hydriding	DZO started in 1995 at 3 to 5 ppb, NMCA at EOC 9 was implemented and HWC started in BOC Cy 10, DZO went to 5 to 10 ppb after the HWC was started. Affected fuel was GE13B claddings that failed in their third cycle with burnups of 43-47 MWd/kgU. Rod oxide thickness peaked at lower and upper part of the rods but maximum oxide thickness was found in upper part of the failed rods.
River Bend, Cy 11, 2003	7 rods failed due to CRUD related corrosion.	Water chemistry apparently within specification. Cy 11 - No NMCA but HWC and Zn-injection, also high Cu coolant content was observed. First cycle fuel with burnup ranging from 14.6-19.0 MWd/kgU. Siemens ATRIUM-10 (LTP). All failed rods were on periphery in FA on bladed surfaces (high power positions). Failures and peak oxide thicknesses in span 2 (of peripheral rods) where max. CRUD deposition was noted.
Hatch 1, Cy 21, 2003	PCI related failures in five (5) liner (barrier) FRs	Five duty related FRs failed at 19 months into a 22 month cycle in one cycle GE14 barrier fuel with an estimated burnup of 26 MWd/kgU.
Fitzpatrick, 2004	PCI related failures in two (2) non-barrier fuel	Two duty related failures occurred in non-barrier GE12 assemblies late in their second cycle at a burnup of about 45 MWd/kgU.

8 Cladding performance under accident conditions LOCA and RIA (Peter Rudling)

8.1 Introduction

8.1.1 Loss of Coolant Accident

The design basis Loss of Coolant Accident (LOCA) is a break in a pipe that provides cooling water to the reactor vessel. Analyses are performed for a variety of break sizes and locations to demonstrate that the ECCS can maintain the fuel in a coolable geometry. The limiting break is typically in one of the cold, main coolant pipes of a PWR or one of the intake pipes to the recirculation pump of a BWR.

The LOCA process starts by the decrease and ultimate loss of coolant flow at the same time that the reactor is depressurized (Figure 8-1). The loss of coolant flow decreases heat removal from the fuel, increasing the fuel temperature and causing a significant temperature rise of the cladding. The decrease in system pressure causes an outward pressure differential and a hoop stress in the cladding wall. The result is the plastic deformation, or *ballooning* of the cladding. Ballooning may also result in *fuel relocation*[25] that may impact the cladding temperature as well as the Equivalent Cladding Reacted (ECR[26]) in the later phase of LOCA.

Ballooning of the fuel rods may result in *blockage* of the coolant sub-channel that in turn may impact the fuel coolability. If large fuel clad burst strains occur at the same axial elevation, *co-planar deformation*, in the FA, the coolability may be significantly degraded. Specifically, the clad azimuthal temperature gradient will strongly impact the burst strain. The extent of the ballooning is also dependent on:

- Creep strength of the cladding.
- Stress in the cladding and the corresponding strain rate.
- Temperature and the rate of temperature increase.

Depending on the temperature, the cladding ductility and the rod internal pressure, the cladding will either stay intact or may burst which will allow steam to oxidize the fuel clad inner surface. In addition, some of the hydrogen released by the water/zirconium corrosion reaction inside the burst fuel may be picked up by the cladding resulting in very high local hydrogen concentrations (1000-3000 wtppm H). A fuel cladding with such high hydrogen concentrations will be very brittle even though the cladding is not oxidised at all, i.e. ECR is 0. The fuel clad axial temperature distribution will determine the axial elevation of the ballooned and burst fuel rods in the assembly. The axial and azimuthal fuel clad temperature distribution is a result of the heat transfer mechanisms at the surfaces of the cladding.

[25] Fuel relocation may occur, if during LOCA a section of the fuel rod experiences ballooning, by slumping of fuel fragments from upper location in the ballooned section.
[26] The ECR is defined as the total thickness of cladding that would be converted to stoichiometric ZrO_2 from all the oxygen that are contained in the fuel cladding as ZrO_2, and oxygen in solid solution in the remaining clad metal phase.

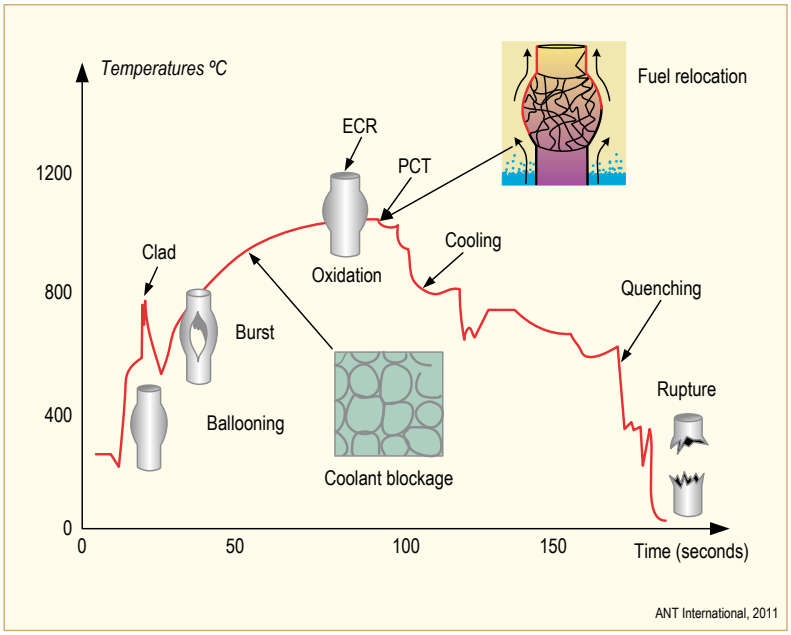

Figure 8-1: Typical LOCA in a PWR.

The increasing temperatures and presence of steam will cause the intact cladding to oxidize on the OD and the burst cladding to oxidize on both the OD and ID (two sided oxidation) until the ECCS is activated and the water quenches the cladding. The oxidation process at the high LOCA temperatures will increase the oxygen and hydrogen content in the cladding, reducing its ductility and resistance to rupture. The process and final structure of the cladding after a LOCA cycle is shown on Figure 8-2:

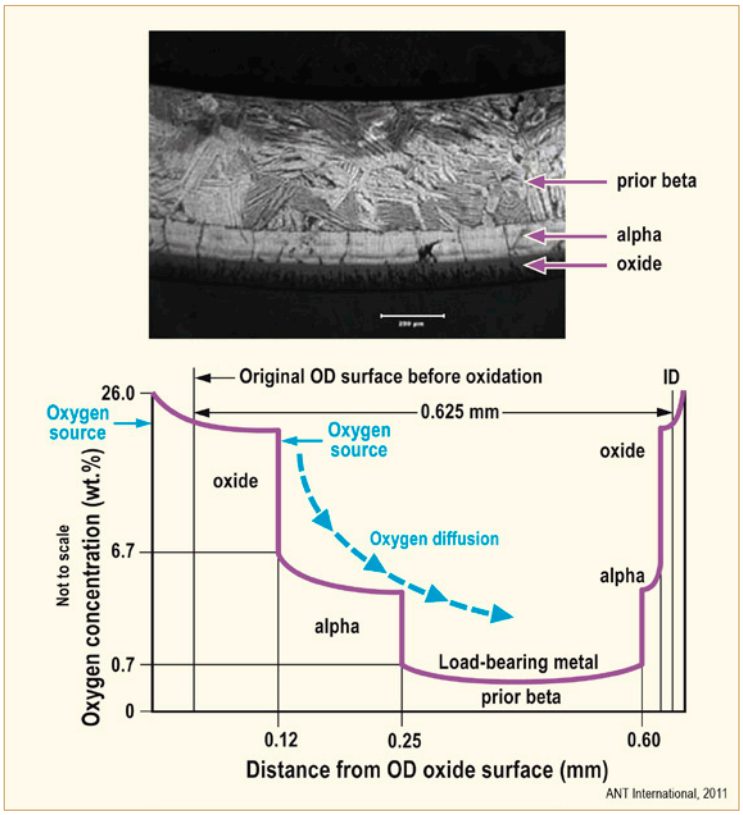

Figure 8-2: Structure of oxidized cladding, after [Meyer, 2013].

- First, the high water and steam temperatures increase their reaction rates with the cladding and increase the conversion of the cladding surface into thicker ZrO_2 films.

- As the LOCA temperature passes the levels where α→β transformations start and finish, the resulting structure consists of:

  – The growing ZrO_2 layer.

  – A brittle zirconium alloy layer with a very high oxygen content which stabilizes the α phase, formed by diffusion of oxygen from the oxide layer.

  – The bulk cladding, which is now in the β phase, has a high solubility for hydrogen; the hydrogen picked up by the cladding from the water-metal reaction increases the solubility of oxygen in the β layer.

- The ZrO_2 and oxygen stabilized α layers grow with continued diffusion of oxygen and hydrogen from the water reaction. The increasing amount of oxygen convert some of the β phase to oxygen stabilized α phase with the concurrent shrinkage of the β phase. The remaining β phase cladding wall thickness is transformed to α phase, or "prior β phase", on cooling and is the only structural part of the cladding that can insure its integrity.

During the LOCA oxidation, the first oxide formed is adherent and protective. However, after an extended exposure, *breakaway oxidation* may occur manifested by the change from parabolic to quasi-linear oxidation kinetics and a dramatic increase in HPUF. High temperature oxidation studies have shown that the Zr-Nb materials M5, ZIRLO have similar LOCA oxidation kinetics compared to that of Zry-4, i.e., an intact black oxide layer is preferentially formed which is associated with low HPUF. However, the Russian Zr-Nb alloys E110 and E635 (with similar chemical compositions to that of M5 and ZIRLO) show a much larger tendency to breakaway oxidation and high hydrogen pickup. It appears that the reason for this difference in behaviour is related to that different source material for E110/E635 (iodide/electrolytic Zr) and M5/ZIRLO (Zr sponge) are used. Also, another reason for the difference in behaviour between these two groups of materials is that the clad outer surface is HF pickled for E110/E635 materials while belt-polishing is used for M5/ZIRLO materials.

The sources and role of hydrogen in the embrittlement of the cladding includes hydrogen from the corrosion reaction during normal operation and hydrogen from the reaction with steam during the LOCA. In addition hydrogen increases the solubility of oxygen and diffusivity of oxygen in the β phase at high temperatures. Oxygen, in combination with hydrogen, are the two major elements that cause cladding embrittlement by the growth of the α layer and the shrinkage of the structural, prior β layer.

Integrity of the cladding is based partly on the properties of the former β zone, since the ZrO_2 and oxygen stabilized α zones are too brittle to sustain a load. The embrittlement criteria are based on properties of the prior β layer measured on post-simulated LOCA tests of unirradiated Zircaloy-4, by ring compression tests [Hobson & Rittenhouse, 1972] and related to oxidation, or ECR, calculated by the Baker-Just equation. It should be noted that the oxide thickness of the samples were never actually measured during those tests. The United States Nuclear Regulatory Commission (USNRC) accepts ECR calculations by the Cathcart-Pawel equation or others that may be submitted for approval.

9 Delayed Hydride Cracking (DHC) during dry storage (David Franklin)

9.1 Introduction

Dry storage of SNF has become a topic of increased interest over recent years as expected dry-storage times have increased to hundreds of years, in large part due to the delays in developing disposal repositories. Delayed hydride cracking (DHC) is a potential failure mechanism for spent nuclear fuel (SNF) [Coleman & Machiels, 2011]. The interest in DHC increases as dry-storage time increases because DHC is time dependent, resulting in the preparation of this section. There are two new products of this section. The primary product is the Section 9.5 analysis of DHC during dry storage based on the USA Surrey ≈15-year dry-storage surveillance program and on test data for DHC velocities and threshold stress intensity factors. That analysis provides a method using the ≈15-year data to analyse the longer times by considering whether there is a time-independent reason why DHC was not observed by ≈15years. The secondary product is a group of variations from the existing DHC methodologies. These variations were developed while performing this analysis of DHC in dry storage. Before describing these two products, the basis for DHC will be reviewed briefly to support the two products. Section 4.3 in ZIRAT15/IZNA10 by C. E. Coleman provided a comprehensive discussion of the DHC process, which will not be reproduced here. Also, comprehensive DHC reviews were published recently by [McRae et al, 2010] and [Puls, 2009].

DHC of zirconium-alloy structural materials has the potential to weaken or fail components. DHC occurs between ambient temperature up to ≈200°C on heating or cooling. Between ≈200°C and ≈350°C DHC occurs only after cooling. DHC occurs faster and over a broader temperature range after monotonic cooling and after thermal cycling to higher temperatures. These conditions exist in dry storage of spent nuclear fuel (SNF). Therefore, DHC during dry storage needs to be understood.

The discussion here will first provide background information, as outlined in Table 9 1. Selected DHC terminology and concepts will be described in Section 9.2. Section 9.3 will list the important dry-storage conditions that are relevant to DHC and that result in the concern for DHC during dry storage. Thereafter, the discussions become more technical and then application oriented. Section 9.4 will recall some fundamental aspects of the DHC process and describe some variations on and expansions from the ZIRAT15/IZNA10 discussion and literature models where appropriate, as outlined in Table 9 1. Sections 9.1.5 and 9.5 provide the two products, both of which are new. The first product in Section 9.1.5 is several model variations that are built principally on the [McRae et al, 2010] version of the DHC Diffusion-First Model (DFM). The second and primary product is the Section 9.5 analysis of the USA Surrey ≈15-year surveillance results, using measured DHC velocity data in the literature, to establish an expectation that DHC will not occur during dry storage because $K_I<K_{IH}$. Thereafter, Section 9.6 provides a brief discussion of the alternative DHC model, termed in the literature the Precipitation-First Model (PFM). This PFM discussion is not provided to support the PFM; it is provided because the primary PFM supporter has associated the PFM with DHC during dry storage. Finally, Section 9.7 will summarize the conclusions and suggest that additional work focus on a new surveillance program that covers the important variables associated with long-term dry storage.

This Section 9 discussion is a summary of the DHC discussion that will be provided in the March 2014 ANT International seminar on dry storage and the subsequent handbook on dry storage, both of which will provide more details on DHC during dry storage as one of many topics on dry storage.

Table 9 1: Outline for discussion on DHC during dry storage.

- DHC conditions during dry storage: Section 9.3
- DHC per Diffusion-First Model (DFM): Sections 9.2 and 9.4
  - High-level concepts
  - Thermal aspects of DHC
  - Stress gradients and thermal interactions
  - Variations from DFMs
- DHC during dry storage: Section 9.5
  - Analysis of expectation for DHC during dry storage: Section 9.1.7
  - Effects of thermal cycling: Section 9.1.8
- Alternative Precipitation-First Model (PFM) for DHC: Section 9.6
- Open items and Conclusions: Section 9.7

ANT International, 2013

9.2 Terminology

Some DHC terminology may not be familiar. In addition, some DHC terminology varies throughout the DHC literature and can cause confusion. Finally, one term is coined here. This section describes selected terminology for clarification. [Puls, 2009] provides definitions for some terms and many of those are used here with the intent to avoid creating new definitions, which would add to the confusion. Beginning with the energies associated with hydrogen in the alpha zirconium and hydride, [Puls, 2009] Section 2, 3rd paragraph provides descriptions of the important interaction and accommodation energies that are associated with (1) the work done by external stresses as volume changes occur, which results in interaction energies and (2) work done as deformation occurs during formation of the hydride phase in the Zr matrix, which results in accommodation energy.

Accommodation energy: Internal energy change to accommodate the volume expansion that occurs. This energy is in the forms of both elastic strain energy and plastic deformation in the alpha matrix and the hydride matrix when some alpha Zr matrix transforms into hydride.

C(a): [H] in highly stressed region, usually the crack-tip region

C(b): [H] in lowly stressed region, usually the bulk region far from the crack tip

C_P: Concentration at which hydrides precipitate

C_D: Concentration at which hydrides dissolve

DFM: Diffusion-First Model

DHC: Delayed Hydride Cracking

DSCS: Dry-Storage Cask System

[H]: Hydrogen concentration

[H]: **Diffusible hydrogen concentration, or diffusible [H]:** The redistribution of hydrogen is related to the hydrogen concentration that is in solution in the alpha-zirconium lattice and is free to migrate to neighbouring lattice positions. The diffusible [H] excludes any hydrogen that is in precipitates or that is in the alpha-zirconium lattice but is tightly bound locally, for example, to sites with oxygen.

[H]: **In-solution hydrogen concentration, or in-solution [H]:** Total hydrogen concentration in solution in a phase, usually in the alpha-zirconium phase as used here. The in-solution [H] includes any hydrogen at traps in the alpha phase and not readily diffusible. The difference between the in-solution [H] and the diffusible [H] probably is small so that either term can be used.

Hydrogen interaction energy: work done by an external applied stress when a hydrogen atom (usually when a mole of hydrogen atoms) is incorporated into either the Zr alpha matrix or the hydride phase; similarly for the reverse process.

Hydride interaction energy: work done by an external applied stress when some alpha Zr matrix transforms into hydride; similarly for the reverse process.

Hydrogen solubility: Solubility is the maximum in-solution [H] in a phase, usually in the alpha-zirconium phase. Solubility is distinct from diffusible or in-solution [H], which often are less than the solubility. Solubility is determined by the Terminal Solid Solubility concentration for Precipitation, designated TSSP, or C_P in its equivalent concentration form. The dissolution boundary, TSSD, does not represent solubility but the concentration - temperature trajectory at which hydrides will dissolve and increase the in-solution [H]. Due to the accommodation energy separating TSSP and TSSD, the conditions for precipitation solubility and dissolution are separated, creating what is termed the hysteresis.

[H] **supersaturation**: In-solution [H] greater than C_P, which is a nonequilibrium condition that will be relieved by hydride precipitation: [Different definition from PFM, for which the definition is not clear but may be similar to C_P - C_D]

K_I: Stress intensity factor (see Figure 9-16)

K_{IH}: Threshold stress intensity factor for DHC (see Figure 9-16)

K_{IC}: Stress intensity factor required for rapid unstable crack propagation (see Figure 9-16)

MOX: Mixed-oxide fuel

PFM: Precipitation-First Mode

SNF: Spent Nuclear Fuel

Solubility: The concentration of hydrogen at which hydrides will precipitate with any additional hydrogen added.

σ_H: Hydrostatic stress at crack tip (a) or in bulk (b)

T_{EQ}: Temperature at which DHC arrests on heating, based on DFM aspect of $C(a)-C(b)=C_P-C_D$ (see Eq. 9-15 through Eq. 9-17 in Section 9.1.1.2).

10 Trends and needs

Improved fuel reliability and operating economics are the driving forces for changing operating conditions, while at the same time maintaining acceptable margins to operating and regulatory safety limits. Table 10-1 gives the trends for BU achieved compared to regulatory limits in various countries. An approximate ("rule of thumb") conversion of BU to fluence is 50 GWd/MT is equivalent to about $1x10^{22}$ n/cm^2, E>1 MeV (or about 17 dpa), but this depends on many nuclear parameters such as enrichment, extent of moderation and neutron energy spectrum. In general PWRs operate to higher discharge BUs compared to BWR because of higher PWR power densities and neutron fluxes, but the differences are decreasing with time. There are some incentives to reach BUs of 60-70 GWd/MT batch average, but the economic values of doing so are decreasing. A majority of US plants and many in Europe have undergone power uprates, from a few percent to up to 20%. This increases the number of FAs in a core that operates at high power, thereby decreasing the margin to established limits. In cooperation with utilities, fuel suppliers have operated LTA or LUAs to very HB, in some cases approaching 100 GWd/MT peak rod exposures.

Table 10-1: Maximum BUs achieved vs. regulatory limits, (excludes LTAs).

	BU (GWD/MT)				
Country	**Batch**	**Assembly**	**Rod**	**Pellet**	**Regulatory limit**
USA	54	58	62	73	62.5 peak rod
Belgium		50-55			55 UO_2 assy., 50 MOX assy.
Czech Republic	51	56	61		60 peak rod
Finland	45.6	46.5	53		45 assy
France	47	51 UO_2 42 MOX			52 assy
Germany	58	62	68		65 assy
Hungary		50	62		
Japan	50	55	62		55 UO_2 assy., 45 MOX assy.
Korean Republic	46				60 rod
Netherlands	51.5	58	64.5		60 rod
Russia	60	65			
Spain	50.4	57.4	61.7	69	
Sweden	47	57.2	63.6		60 assy., 64 rod
Switzerland	58	60	65	71	80 pellet
Taiwan					60 rod (P), 54 assy. (B)
UK	44.3	46.5	50		55 pellet
Ukraine		50			

ANT International, 2011

11 References

10 CFR Part 50 Appendix A, *General Design Criteria for Nuclear Power Plant*s, U.S., Government Printing Office, Washington, 1990.

10 CFR Part 100.11, *Determination of Exclusion Area, Low Population Zone, and Population Centre Distance*, U.S. Government Printing Office, Washington, 1990.

Abolhassani S et al, *Corrosion and hydrogen uptake in Zirconium claddings irradiated in light water reactors*, 17th International Symposium on Zirconium in the Nuclear Industry, Hyderabad, India, 2013.

Adamson R., Garzarolli F., Patterson C., Rudling P., Strasser A., Coleman K. and Lemaignan C., *ZIRAT16/IZNA11 Annual Report*, ANT International, Mölnlycke, Sweden, 2011.

Allen V. et al, *Study of Zircaloy corrosion to develop mechanistic understanding*, 17th International Symposium on Zirconium in the Nuclear Industry, Hyderabad, India, 2013.

Anada H. and Tekada K., Microstructure of oxides on Zircaloy-4, 1.0Nb Zry-4, and Zircaloy-2 formed in 10.3-MPa steam at 673°C, ASTM STP 1295, pp. 34-54, 1996.

Anada H. et al, *Effect of annealing temperature on corrosion behaviour and ZrO_2 microstructure of Zry-4 cladding tube*, ASTM STP 1295, pp. 74-93, 1996.

Arashi H. and Ishigame J. M., Raman spectroscopy studies of the polymorphism in ZrO_2 at high stresses, Phys. Stat. Sol. 71, 313, pp. 313-321, 1982.

Arkoma A., Tulkki V., *Release of radioactive nuclides from spent WWER fuel*, VVER conference in 2013, to be published

Asatiani I., Balabanov S. and Kuznetsov A., *Operational Results of WWER Fuel Fabricated by MSZ, (Elektrostal, Russia)*, VVER Fuel Performance Conference, Helena Resort, Bulgaria, September, 2011.

Barbéris P., *Zirconia powders and Zircaloy oxide fils: tetragonal phase evolution during 400°C autoclave tests*, J. Nucl. Mat. 226, pp. 34-43, 1995.

Bare W. and Torgerson L., *Dry Cask Storage Characterization Project – Phase 1: CASTOR v/21 Cask opening and Examination*, INEEL/EXT-01-00183, Rev. 1. August, 2001.

Beie H. J. et al, *Examination of the corrosion mechanism of Zr alloys*, ASTM STP 1245, pp. 615-643, 1994.

Billone M. C., Yan Y., Burtseva T. A. and Daum R., *Cladding Embrittlement during Postulated Loss-of-Coolant Accidents*, NUREG/CR-6967, 2008. [ML082130389 at http://www.nrc.gov/reading-rm/adams.html]

Billone M. C., *Assessment of Current Test Methods for Post-LOCA Cladding Behaviour*, NRC report NUREG/CR-7139, 2012.

Billone M. C., Burtseva T. A. and Yan Y., *Ductile-to-Brittle Transition Temperature for High-Burnup Zircaloy-4 and ZIRLO Cladding Alloys Exposed to Simulated Drying-Storage Conditions*, NRC Report No. ML12181A238, September 28, 2012.

Billone M. C., Burtseva T. A. and Einziger R. E., *Ductile-to-brittle transition temperature for high-burnup cladding alloys exposed to simulated drying-storage conditions*, Journal of Nuclear Materials 433, 431–448, 2013.

Bouineau V. et al, *A New Model to Predict the oxidation kinetics of Zr alloys in PWR*, 15th ASTM Internat. Symp. On Zr in the Nucl. Industry, Sunriver, Or. USA, 2007.

Bossis P. Lelievre G., Barberis P., Iltis X. and LeFebvre F., *Multi-Scale Characterisation of the Metal-Oxide Interface of Zirconium Alloys*, Proc. 12th Int. Symp. on Zr in the Nucl. Ind., ASTM-STP-1354, pp. 918-940, 2000.

Bossis P., Thomazet J. and Lefebvre F., *Study of the Mechanisms Controlling the Oxide Growth Under Irradiation: Characterization of Irradiated Zircaloy-4 and Zr-1Nb-O Oxide Scales*, Zirconium in the Nuclear Industry: Thirteenth International Symposium: ASTM STP 1423, G. D. Moan and P. Rudling, Eds., ASTM International, pp. 190-221, West Conshohocken, PA, 2002.

Bossis P., Verhaeghe B., Doriot S., Gilbon D., Chabretou V., Dalmais A., Mardon J. P., Blat M. and Miquet A., *In PWR Comprehensive Study of High Burn-up Corrosion and Growth Behaviour of M5 and Recrystallised Low-Tin Zircaloy-4*, 15th ASTM International Symposium: Zirconium in the Nuclear Industry, ASTM I, STP 1505, pp. 430-456, Sunriver, OR, June 25-27, 2009.

Bradhurst D.H. and Heuer P.M., *The influence of oxide stress on the breakaway oxidation of Zircaloy-2*, J. Nucl. Mat. 37, pp. 35-37, 1970.

Broy Y., Garzarolli F., Seibold A. and Van Swam L. F., *Influence of transition elements Fe, Cr, and V on long time corrosion in PWRs*, Zirconium in the Nuclear Industry: 12th Int'l Symposium, ASTM STP 1354, pp. 609-622, G. P. Sabol and G. D. Moan, Eds., West Conshohocken, PA, 2000.

Cann C. D. and Sexton E. E., *An electron optical study of hydride precipitation and growth at crack tips in zirconium*, Acta Met., 28, 1215-1221, 1980.

Cantonwine P., Paustian H., Hahn G. and Tusar J., *Channel – Control Blade Interference in GE Boiling Water Reactor, D-Lattice Plants with Zircaloy-2 Channels*, Michael Reitmeyerd, and Erik Mader, LWR Fuel Performance Meeting/TopFuel/WRFPM, Paper 079, Orlando, Florida, USA, September 26-29, 2010.

Cantonwine P. E., Lin Y-P., Lutz D. R., White D. W. and Ledford K. L., *BWR Corrosion Experience of NSF Channels*, LWR Fuel Performance Meeting / Top Fuel 2013, Charlotte, NC, USA, September 15-19, 2013.

Carmack J., Goldner F., Bragg-Sitton S. M and Snead L. L., *Overview of the U.S. DOE accident tolerant fuel development program*, TopFuel, 2013.

Carpenter G. J. C., Zee R. H. and Rogerson A., J. Nucl. Mater. 159, pp. 46, 1988.

Chapin D. L., Brashier R.W., Staub D. E., O'Cain M. B., Höglund J. S., Jasiulevicius A., Josefsson B., and Miguel Aulló, *Design and Operation of EFG Fuel in Ringhals PWRS*, Top Fuel, 2013.

Charquet D. et al, *Hydrogen absorption kinetics during Zircaloy oxidation in steam*, ASTM STP 1245, pp. 80-97, 1994.

Cheadle B. A., Coleman C. E., Ambler J. F. R., *Prevention of delayed hydride cracking in zirconium alloys*, ASTM STP 939, Zirconium in the Nuclear Industry – Seventh International Symposium, R. B. Adamson and L. F. P. Van Swam, Eds., American Society for Testing and Materials, 224-240, Philadelphia, PA., 1987.

Cheng B., Krüger R. M. and Adamson R. B., *Corrosion Behaviour of Irradiated Zircaloy*, Proc. 10th Int. Symp. in the Nucl. Ind., ASTM-STP-1245, pp. 400-418, 1994.

Cheng B., *Fuel behaviour in severe accidents and Mo-alloy based cladding designs to improve accident tolerance*, Top Fuel, 2012.

Cheng B., Kim Y-J., Chou P. and Deshon J., *Development of Mo-alloy for LWR fuel cladding to enhance fuel tolerance to severe accidents*, TopFuel, 2013.

Nomenclature

AFA	Advanced Fuel Assembly
ANL	Argonne National Laboratory
AO	Axial Offset
AOA	Axial Offset Anomaly
AOO	Anticipated Operational Occurrence
AREVA	French Equipment Manufacturer
ASI	Axial Shape Index
ASTM	American Society for Testing and Materials
ATF	Accident Tolerant Fuels
ATR	Advanced Test Reactor
B&W	Babcock & Willcox
BF	Browns Ferrry
BOC	Beginning of Cycle
BQ	Beta-Quenched
BU	Burnup
BW	Basket-Weave
BWR	Boiling Water Reactor
CANDU	Canadian Deuterium Uranium
CE	Combustion Engineering
CEA	Commissariat à l'Energie Atomique
CFD	Computational Fluid Dynamic
CFR	Code of Federal Regulations
CGG	Columnar Grain Growth
CILC	CRUD Induced Localised Corrosion
CIM	Channel Interference Metric
CIPS	CRUD Induced Power Shift
CP	Cathcart-Pawel
CPR	Critical Power Ratio
CR	Control Rod
CRP	Coordinated Research Project
CRUD	Chalk River Unidentified Deposits
CT	Central Tube
CVI	Chemical Vapour Infiltration
CWSR	Cold Work and Stress Relieved
DCP	Distinctive CRUD Pattern
DFM	Diffusion-First Model
DHC	Delayed Hydride Cracking
DNB	Departure from Nucleate Boiling
DNBR	Departure from Nucleate Boiling Ratio
DSC	Differential Scanning Calorimetry
DSCS	Dry-Storage Cask System
DX	Duplex
DZO	Depleted Zinc Oxide
ECBE	Effective Control Blade Exposure
ECC	Emergency Core Cooling
ECCS	Emergency Core Cooling System
ECR	Equivalent Cladding Reacted
EdF	Electricité de France
EDS	Energy Dispersive Spectroscopy
EELS	Electron Energy Loss Spectroscopy
EFG	European Fuel Group
EFID	Effective Full Insertion Days
EFPD	Effective Full Power Days
EGG	Equiaxed Grain Growth
ELS	Extra-Low Sn
EOC	End Of Cycle